



UNIVERSITY OF
LIVERPOOL

UNIVERSITY OF LIVERPOOL

**Mathematical Study of Biochemical
Reactions with Application to the Sonic
Hedgehog Signalling System**

Thomas Malone

Supervisor: Dr. Bakhtier Vasiev

Submitted to the Department of Mathematical Sciences in partial fulfilment of
the requirements for the degree of Master of Mathematics

May 26, 2015

Contents

Introduction	1
1 Michaelis-Menten Kinetics	3
1.1 Michaelis-Menten Equation	3
1.2 Quasi Steady State Assumption	6
1.3 Nondimensionalisation	8
2 Cooperative Phenomena	13
2.1 Simple Derivation of Sigmoidal Kinetics	13
2.2 Cooperative Reactions with Intermediate Steps	15
3 Positive and Negative Feedback Systems	19
3.1 Yeast Glycolytic Oscillations	20
3.2 Bistability: Mutual Activation and Mutual Inhibition	25
4 The Sonic Hedgehog (Shh) Signalling System	31
4.1 Introduction to the Shh Pathway	31
4.2 Shh Mathematical Model	33
4.3 Derivation of Signal	36
4.4 Shh as a Bistable Switch	37
4.5 Bifurcation Analysis of Disease Causes Within the Shh Network	39
4.5.1 Gene Amplification of <i>gli1</i>	39
4.5.2 Ptc and Smo Mutations	40
4.5.3 Gli3 Truncations	40
5 Shh and Development of the Spinal Cord	42
5.1 Spinal Cord Ventral Patterning	42
5.2 Revised Model of Core Shh Signalling System	43
5.3 Parameter Values and their Effects	45
5.4 Model including FGF signalling	48
6 Conclusion	51

Introduction

This project is dedicated towards the mathematical modelling of dynamics of biochemical reactions, with an emphasis on the Sonic Hedgehog signalling system. Within all living organisms, biochemical reactions occur which affect and determine the outcome of many biological processes. The aim of the project is to further understand how we are able to model such biochemical reactions mathematically by considering two simplified models of Michaelis-Menten kinetics. The reasoning behind mathematically modelling such reactions is to develop an understanding of how they function, what their purpose is and even possibly determine why a reaction may fail to operate in the way it should. We will then see where we are able to simplify the more complicated reactions in order to fit the Michaelis-Menten model and then focus on how we are able to analyse the systems in depth.

We will also look into feedback loops within biological systems, an important feature to regulate reactant and product concentrations. Examples of such we will look into are yeast glycolysis, mutual inhibition and mutual activation which will develop our understanding of the techniques used to analyse said feedback loops. By understanding the mechanics behind a feedback loop, we will be able to determine under what conditions a feedback loop may not work effectively, or correctly.

Using the knowledge gained from the previous examples, we will apply the techniques to the Sonic Hedgehog signalling pathway; an integral signalling system which will aid our understanding of how the spinal cord and brain are formed. By analysing this system, we will aim to understand mathematically how mutations and disease are caused within the system. We will also research whether the system will be stable under specific conditions by using the developed techniques from previous chapters. Lastly, we will look into how the system reacts to the presence of Fibroblast Growth Factors (FGF) and look into whether these systems will change with an increase in FGF concentration.

Chapter 1

Michaelis-Menten Kinetics

1.1 Michaelis-Menten Equation

As every second passes by, biochemical reactions continually occur in all living organisms, in every single living cell. These reactions involve proteins called *enzymes*, which are biological catalysts. During such enzymatic reactions, these catalysts react selectively with a *substrate*, which is then modified into an end product. An example of such is the enzyme *lactase*, catalysing the substrate *lactose* that is digested to produce *glucose* and *galactose*. Without an understanding of enzymatic reactions, we could not conclude that lactose intolerance is due to a lactase deficiency. A basic enzymatic reaction, proposed by biochemist Leonor Michaelis and physician Maud Menten (1913), involves a substrate, S reacting with an enzyme, E to form a substrate-enzyme complex, SE , which is then converted into a product, P and the enzyme, E . This can be represented by:



where rate constants k_1, k_{-1} and k_2 (the constants of proportionality), dictate the rates at which these reactions occur. That is, S and E combine at a constant rate k_1 to form SE . However, as this reaction is reversible (indicated by the double arrows), the complex SE can break down into the former constituents. In addition, the complex SE can produce P and E , at a constant rate of k_2 which is not reversible (indicated by the single arrow). This reaction is in fact reversible, however, products very rarely go back to form reactants as the forward reaction is usually thermodynamically stable. To paint a picture in our mind, imagine a cell with membrane receptors (enzymes), which is surrounded by nutrient molecules (substrates) as shown in Figure 1.1. The idea is that we want to transfer nutrients from outside the cell, through the cell membrane via the receptors, and then into the cell. Due to the limited amount of receptors and limited rate at which they can catalyse the reaction, saturation occurs. This is the maximal rate at which the reaction can take place. From (1.1), one molecule of S combines with

one molecule of E to produce one of SE . This then produces one molecule of P and one molecule of E . We also need a way of defining the reactions in terms of concentrations and this can be done with *The Law of Mass Action*.

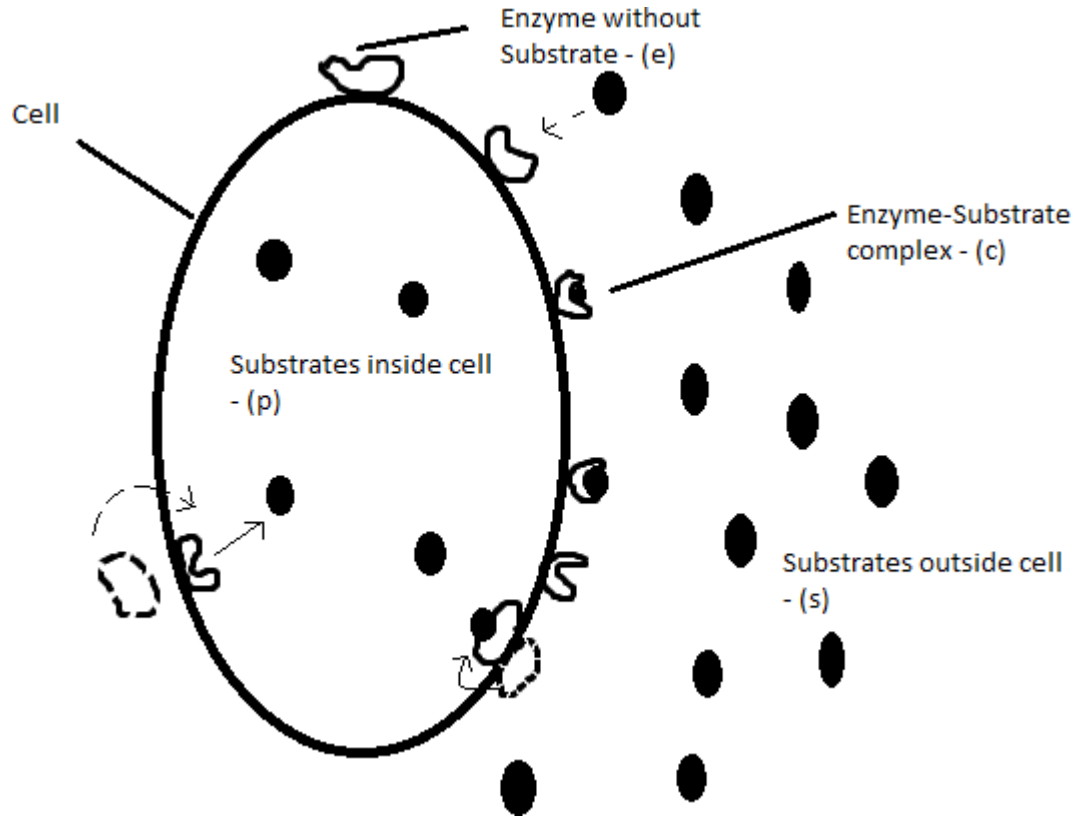


Figure 1.1: The saturation mechanism for substrate uptake into cells can be described by Michaelis-Menten Kinetics.

Definition 1.1.1. The Law of Mass Action: The rate of a reaction is *proportional* to the product of the concentrations of the reactants.

Let lowercase letters denote the concentrations of the reactants in (1.1)

$$s = [S], e = [E], c = [SE], p = [P] \quad (1.2)$$

where [...] brackets denotes concentration. We must have initial conditions, which are

$$s(0) = s_0, e(0) = e_0, c(0) = 0, p(0) = 0 \quad (1.3)$$

This is due to the initial amount of enzymes and substrates at $t = 0$, hence there are no enzyme complexes formed, nor any product. In order to mathematically model this reaction, we can now apply The Law of Mass Action to (1.1) to obtain a system of non-linear reaction equations. Using (1.2), we can write these equations in the following way:

$$\frac{ds}{dt} = -k_1se + k_{-1}c \quad (1.4a)$$

$$\frac{de}{dt} = -k_1se + (k_{-1} + k_2)c \quad (1.4b)$$

$$\frac{dc}{dt} = k_1se - (k_{-1} + k_2)c \quad (1.4c)$$

$$\frac{dp}{dt} = k_2c \quad (1.4d)$$

Let us analyse these equations. Combining(1.4b)(1.4c), we obtain the following equation:

$$\frac{de}{dt} + \frac{dc}{dt} = 0 \quad (1.5)$$

This is a very common feature of many enzymatic reactions. It tells us that $e + c$ is a *constant*, which by relating to a biological viewpoint, the total amount of substrate-free enzymes and enzyme-substrate complexes is constant. This is due to the fact that no enzyme is destroyed during the process. If we consider the amount of initial enzymes, e_0 , then due to our equation, over time this total amount will still remain as e_0 . Hence, we can consider this as

$$e + c = e_0 \quad (1.6)$$

Using (1.6) we may now simplify further the system of equations by eliminating e or c . Arbitrarily we choose to eliminate e . As (1.4a), (1.4b) and (1.4c) are not dependent on concentration p , we can exclude (1.4d) for now, which can later be solved once solutions for other variables are known. Let $e = e_0 - c$ and substitute into (1.4a), (1.4b) and (1.4c)

$$\frac{ds}{dt} = -k_1(e_0 - c)s + k_{-1}c = -k_1se_0 + (k_1s + k_{-1})c \quad (1.7a)$$

$$\begin{aligned} \frac{de}{dt} &= -k_1(e_0 - c)s + (k_{-1} + k_2)c = -k_1se_0 + (k_1s + k_{-1} + k_2)c \\ &= \frac{d(e_0 - c)}{dt} = -\frac{dc}{dt} \end{aligned} \quad (1.7b)$$

$$\frac{dc}{dt} = k_1(e_0 - c)s - (k_{-1} + k_2)c = k_1se_0 - (k_1s + k_{-1} + k_2)c \quad (1.7c)$$

with initial conditions

$$s(0) = s_0, c(0) = 0 \quad (1.7d)$$

1.2 Quasi Steady State Assumption

In this section, we fixate on an assumption that will direct us to the Michaelis-Menten rate law, and conclude the restrictions to which the assumption is not applicable. In most cases, substrates are found to be in a much higher concentration than the concentration of enzymes. Thus, we are able to argue that the enzymes are working at maximal capacity, so there is almost always a substrate occupying an enzyme. This assumption implies the following equation:

$$\frac{dc}{dt} \approx 0 \Rightarrow k_1 e_0 s - (k_1 s + k_{-1} + k_2) c = 0 \quad (1.8a)$$

This is called the *quasi steady state assumption*, from which we can have an equation for c in terms of s ,

$$c = \frac{k_1 e_0 s}{k_1 s + k_{-1} + k_2} = \frac{e_0 s}{s + K_m} \quad (1.8b)$$

where $K_m = \frac{k_{-1} + k_2}{k_1}$

By substitution into (1.7a) we obtain the following:

$$\begin{aligned} \frac{ds}{dt} &= -k_1 e_0 s + \left(k_1 s + k_{-1} \right) \frac{e_0 s}{s + K_m} \\ &= \left(-k_1 \left(s + \frac{k_{-1} + k_2}{k_1} \right) + k_1 s + k_{-1} \right) \frac{e_0 s}{s + K_m} \\ &= \left(-k_1 \left(\frac{k_{-1} + k_2}{k_1} \right) + k_{-1} \right) \frac{e_0 s}{s + K_m} \\ &= \left(-k_{-1} - k_2 + k_{-1} \right) \frac{e_0 s}{s + K_m} \\ &= \frac{-k_2 e_0 s}{s + K_m} = -\frac{V_{max} s}{s + K_m} \end{aligned} \quad (1.8c)$$

where K_m is called the Michaelis constant and $V_{max} = k_2 e_0$. When using (1.8a), we

can assume that the change in product is equal to the change substrate concentration. That is:

$$\frac{dp}{dt} = -\frac{ds}{dt} \Rightarrow \frac{dp}{dt} = \frac{V_{max}s}{s + K_m} \quad (1.8d)$$

Using the result (1.8c), it is possible to illustrate what is happening in the reaction over time. The graph of rate of product formation versus substrate concentration shows how the michaelis-menten equation evolves. Let us say that we had a limited number of enzymes and so for a smaller substrate concentration, the rate of product formation is shown to be linear, increasing with a constant rate when s increases. This rate however gradually slows down, as the substrate concentration becomes closer to that of the enzyme concentration. When s becomes greater than e however, the rate of product formation cannot increase anymore, hence we obtain V_{max} , shown on Figure 1.2 below. The approximate dynamics of the reaction is shown in (1.8c), known as the *quasi steady state assumption*.

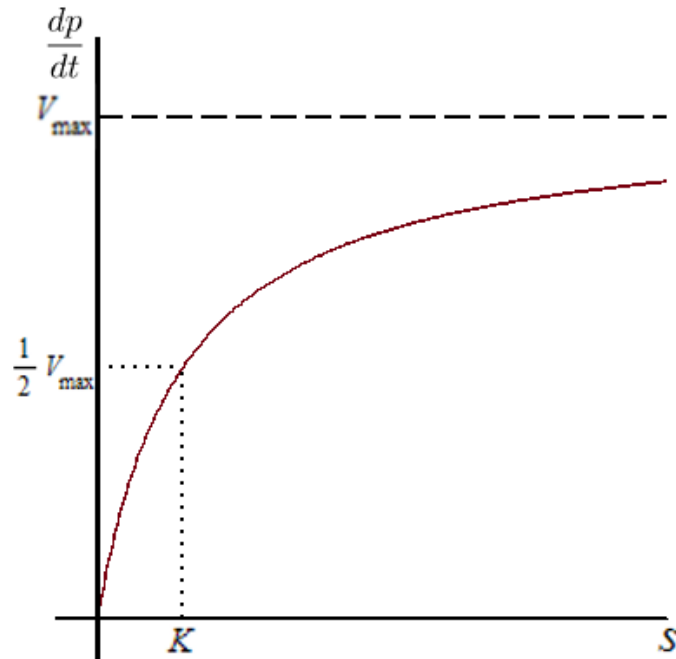


Figure 1.2: Graph of the rate of product formation, $\frac{dp}{dt}$ versus substrate concentration, s . The curve levels off towards a maximal rate V_{max} as s increases. At a substrate concentration level, K , the rate of production is exactly half of the maximal rate, $\frac{1}{2}V_{max}$.

This means that whenever we have type of reaction occurring, with an enzyme catalysing the reaction of substrate into a product, we are able to assume that the ODEs that represent a specific system, may now be represented in a way similar to (1.8c), which is a very important, time efficient tool to have.

We may take the assumption that the enzyme has a concentration much lower than the substrate concentration, so the substrate concentration does not change during the initial transient stage of the reaction. Using the initial condition that $s(0) = s_0$, we may use (1.8c) by solving the differential equation implicitly.

$$\begin{aligned} \frac{s + K_m}{s} ds &= k_2 e_0 dt \\ \Rightarrow \int \left(1 + \frac{K_m}{s}\right) ds &= - \int k_2 e_0 dt \\ \Rightarrow s + K_m \ln s &= -k_2 e_0 t + A \end{aligned}$$

Where A is a constant. Using the initial condition, $s(0) = s_0$,

$$\Rightarrow s + K_m \ln s = -k_2 e_0 t + s_0 + K_m \ln s_0 \quad (1.8e)$$

We may now substitute this solution into (1.8b) to obtain an expression for the complex $c(t)$. However, due to the initial condition on $c(0) = 0$, the condition would not be satisfied. To get past this problem, it is required to split the timescale in two: the initial time scale near $t = 0$, while the second is the longer timescale, where there is a significant change to the substrate concentration during which it's possible to approximate the enzyme-substrate complex concentration by (1.8b) using $s(t)$ from (1.8e).

1.3 Nondimensionalisation

To proceed further, it is preferred to reduce the equations (1.7a) and (1.7c) together with (1.7d) into dimensionless form. The reason to do this is because it reduces the number of times we might have to solve the equation numerically. In addition to this, it gives an insight into what might be small parameters that could be ignored or approximated. Generally, it is done so that it is easier to analyse. Firstly, we introduce dimensionless quantities;

$$\begin{aligned} \tau = k_1 e_0 t, u(\tau) = \frac{s(t)}{s_0}, v(\tau) = \frac{c(t)}{e_0} \\ \lambda = \frac{k_2}{k_1 s_0}, K = \frac{k_{-1} + k_2}{k_1 s_0} = \frac{K_m}{s_0}, \epsilon = \frac{e_0}{s_0} \end{aligned} \quad (1.9)$$

where we claim $\epsilon \ll 1$ due to the assumption that initial substrate concentration is much greater than initial enzyme concentration. Note the time scale chosen. There are actually two different time scales in which the reaction occurs. The first timescale

chosen is the ‘long timescale’, occurring over the duration of the reaction after all enzyme active sites are initially filled with substrates. The second timescale is the ‘short timescale’ where it covers the reaction occurring over the initial period when the substrate reacts with the enzymes near $t = 0$. To identify which timescale is long or slow, notice that $\epsilon \ll 1$, which implies that $s_0 \gg e_0$. Hence, for our two time scales τ and $\tilde{\tau}$, we see that $\tau \gg \tilde{\tau}$ and so we can claim that τ is for the longer timescale. Continuing with the ‘long timescale’, and by substitution into (1.7a)(1.7c) we obtain the dimensionless system of equations for the quasi steady state approximation. From $\tau = k_1 e_0 t$ we see that;

$$\frac{d}{dt} = \frac{d\tau}{dt} \frac{d}{d\tau} = k_1 e_0 \frac{d}{d\tau} \quad (1.10)$$

which we may substitute into (1.7a) and (1.7c). From (1.9), we can replace $s(t)$ and $c(t)$ in (1.7a)(1.7c) with dimensionless quantities, and so becomes:

$$\begin{aligned} k_1 e_0 s_0 \frac{du}{d\tau} &= -k_1 e_0 s_0 u + (k_1 s_0 u + k_{-1}) e_0 v \\ \Rightarrow \frac{du}{d\tau} &= -u + \left(u + \frac{k_{-1}}{k_1 s_0}\right) v \\ \Rightarrow \frac{du}{d\tau} &= -u + (u + K - \lambda) v \end{aligned} \quad (1.11a)$$

$$\begin{aligned} k_1 e_0^2 \frac{dv}{d\tau} &= k_1 e_0 s_0 u - (k_1 s_0 u + k_{-1} + k_2) e_0 v \\ \Rightarrow \frac{e_0}{s_0} \frac{dv}{d\tau} &= u - \left(u + \frac{k_{-1} + k_2}{k_1 s_0}\right) v \\ \Rightarrow \epsilon \frac{dv}{d\tau} &= u - (u + K) v \end{aligned} \quad (1.11b)$$

From our quasi state state assumption (1.8a), and comparing this to (1.11b), it is equivalent to assume the LHS of equation (1.11b) is also small (approximately zero), that is, $\epsilon \ll 1$. Hence by this assumption, the given equations are:

$$\frac{du}{d\tau} = -u + (u + K - \lambda) v \quad (1.12a)$$

$$0 = u - (u + K) v \quad (1.12b)$$

This implies, by substitution and rearranging that;

$$v = \frac{u}{u + K} \quad (1.13a)$$

$$\begin{aligned} \Rightarrow \frac{du}{d\tau} &= -u + (u + K - \lambda) \frac{u}{u + K} \\ &= -u + u - \frac{\lambda u}{u + K} \\ \Rightarrow \frac{du}{d\tau} &= -\frac{\lambda u}{u + K} \end{aligned} \quad (1.13b)$$

From the original equation (1.1), the final steady states of u and v are both equal to zero, due to the fact that over time, all substrates will convert to products, so there are no substrates or substrate complexes left. By analysis of equation (1.13a), if $u > 0$ then $\frac{du}{d\tau} < 0$ decreases over time. We can integrate (1.13b) to find an equation for the relaxation time (long timescale), which is at the time $u = \frac{1}{e}$

$$\begin{aligned} \int \frac{u + K}{u} du &= - \int \lambda d\tau \\ \Rightarrow u + K \ln(u) &= -\lambda\tau + C \end{aligned}$$

using initial condition, $u(0) = 1 \Rightarrow C = 1$

$$\Rightarrow u + K \ln(u) = -\lambda\tau + 1$$

substitute $u = \frac{1}{e}$:

$$\begin{aligned} \Rightarrow \frac{1}{e} - K &= -\lambda\tau_{RT} + 1 \\ \Rightarrow \tau_{RT} &= \left(1 - \frac{1}{e} + K\right) \frac{1}{\lambda} \end{aligned} \quad (1.14)$$

From this result, we can see that the relaxation time is inversely proportional to λ . That is, from (1.9) as k_2 increases (the rate of product formation), the long timescale for the reaction decreases. Also, from (1.13a) we see that v will decrease as u decreases. To conclude, for the timescale τ , substrate and substrate-enzyme complex concentrations decrease over time. It is possible to increase the accuracy using a technique called singular perturbation method [2].

For the second (short) timescale, by repeating the process done for the long timescale, we choose the same dimensionless quantities as in (1.9), except instead of τ , we now

have the equation:

$$\tilde{\tau} = k_1 s_0 t \quad (1.15)$$

Following the method previously done before, we obtain a new set of equations

$$\frac{du}{d\tilde{\tau}} = -\epsilon u + \epsilon(u + K - \lambda)v \quad (1.16a)$$

$$\frac{dv}{d\tilde{\tau}} = u - (u + K)v \quad (1.16b)$$

As this is during the fast timescale, it would be appropriate to assume that this timescale explains in greater detail how enzymes initially fill their active sites with substrates (near $t = 0$). Using the quasi steady state assumption again, that $\epsilon \ll 1$, the RHS of (1.16a) may be neglected and so we obtain:

$$\frac{du}{d\tilde{\tau}} = 0 \Rightarrow u = \frac{s(0)}{s_0}, \text{ as } s(0) = s_0 \quad (1.17a)$$

Using the assumption above, for this timescale, u is constant, and so we can substitute this into(1.16b) and integrate.

$$\int \frac{dv}{1 - (K + 1)v} = \int d\tilde{\tau}$$

let $w = 1 - (K + 1)v$

$$\begin{aligned} &\Rightarrow \int \frac{dw}{-(K + 1)w} = \int d\tilde{\tau} \\ &\Rightarrow -\frac{\ln(1 - (K + 1)v)}{K + 1} = \tilde{\tau} + C \end{aligned}$$

Using initial conditions, $v(0) = 0 \Rightarrow C = 0$ and by rearranging

$$\Rightarrow v = \frac{1 - e^{-\tilde{\tau}(K+1)}}{K + 1} \quad (1.17b)$$

Knowing that at $\tilde{\tau} = 0$, the enzymes are unoccupied as $v(0) = 0$, for which enzyme-substrate complexes are then formed rapidly until a steady fixed maximal rate is achieved. This in turn will decrease over time due to the loss of substrates outside of the cell. It is possible to use both timescales τ and $\tilde{\tau}$ to analyse what is happening

during the fast transient stage of the reaction, and what is happening during the relaxation period (the longer timescale). Using the $\tilde{\tau}$ timescale, we see that for the transient stage of the reaction, as $\tilde{\tau}$ increases, v tends towards a value of $\frac{1}{K+1}$, which is consistent with the τ timescale, as we concluded that $v = \frac{u}{K+u}$ where $u(0) = 1$.

From here, it is easier to look at the τ timescale, as it gives a more detailed view of the relaxation period of the reaction. We mentioned that from (1.13a), v decreases as u decreases at a rate given by (1.13b), until they both reach a steady state value of zero. This can be shown by the phase portrait below in Figure 1.3:

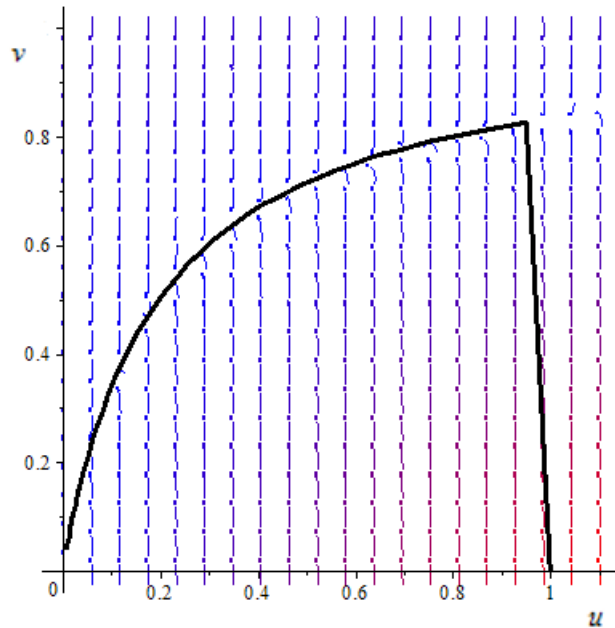


Figure 1.3: Graph of dimensionless quantities of enzyme-substrate complex concentration and substrate concentration respectively, v versus u , showing the fast transition to value of $v = \frac{1}{1+K}$ and then gradually at a slower rate towards zero.

As both timescales have been covered, we must combine the solutions using a technique called *matched asymptotic analysis*, which will not be seen in detail here. However, a figure of the substrate concentration as a function of time using these timescales can be found in the book by Leah Edelstein-Keshet [1]. The results of this technique however gives an insight into the complete image of events for both short and long timescales together.

Chapter 2

Cooperative Phenomena

2.1 Simple Derivation of Sigmoidal Kinetics

For a simple Michaelis-Menten kinetic reaction, the reaction rate increases proportional to the substrate concentration, providing that the level of substrate concentration is low to begin with (near $s = 0$). This is because the chance of a substrate encountering an enzyme increases proportionally. However, the properties of this proportionality changes when we introduce an enzymatic reaction that involves two substrates reacting with the same enzyme:



Similarly to the singular substrate example, it is possible to analyse this in a similar way, with a few minor changes. According to the law of mass action stated in the previous chapter, we conclude that for a reaction that requires two molecules of substrate S to react with one molecule of enzyme E, it must do so at a rate of k_1 . Therefore, we may express the equations of the reaction as follows:

$$\frac{ds}{dt} = -k_1 s^2 e + k_{-1} c \quad (1.19a)$$

$$\frac{de}{dt} = -k_1 s^2 e + (k_{-1} + k_2) c \quad (1.19b)$$

$$\frac{dc}{dt} = k_1 s^2 e - (k_{-1} + k_2) c \quad (1.19c)$$

$$\frac{dp}{dt} = k_2 c \quad (1.19d)$$

With initial conditions: $s(0) = s_0$, $c(0) = 0$. Again, similarly to before we are able to simplify the equations using (1.6) and so we obtain

$$e = e_0 - c \Rightarrow \frac{ds}{dt} = -k_1(e_0 - c)s + k_{-1}c = -k_1se_0 + (k_1s + k_{-1})c \quad (1.20a)$$

$$\frac{dc}{dt} = k_1(e_0 - c)s - (k_{-1} + k_2)c = k_1se_0 - (k_1s + k_{-1} + k_2)c \quad (1.20b)$$

Observing the differences between this double substrate model and the single substrate model, it's clear that the equations (1.20a)(1.20b) are identical to (1.7a)(1.7b) with one minor change, that s has been replaced with s^2 . From here, we are able to govern the rate equation for the substrate concentration, s .

$$\frac{dc}{dt} \approx 0$$

$$\Rightarrow k_1e_0s^2 - (k_1s^2 + k_{-1} + k_2)c = 0$$

$$\Rightarrow c(t) = \frac{k_1e_0s(t)^2}{k_1s(t)^2 + k_{-1} + k_2} = \frac{e_0s(t)^2}{s(t)^2 + K_m} \quad (1.20c)$$

where $K_m = \frac{k_{-1}+k_2}{k_1}$. Now by substitution into (1.20a), we obtain

$$\begin{aligned} \frac{ds}{dt} &= -k_1 \left(e_0 - \frac{e_0s^2}{s^2 + K_m} \right) s^2 + k_{-1} \frac{e_0s^2}{s^2 + K_m} \\ &= -k_1s^2e_0 + \left(k_1s^2 + k_{-1} \right) \frac{e_0s^2}{s^2 + K_m} \\ &= \left(-k_1 \left(s^2 + K_m \right) + k_1s^2 + k_{-1} \right) \frac{e_0s^2}{s^2 + K_m} \\ &= \left(-k_1K_m + k_{-1} \right) \frac{e_0s^2}{s^2 + K_m} \\ &= \left(-k_{-1} - k_2 + k_{-1} \right) \frac{e_0s^2}{s^2 + K_m} \\ &= \frac{-k_2e_0s^2}{s^2 + K_m} = -\frac{V_{max}s^2}{K_m + s^2} \end{aligned} \quad (1.21)$$

where $V_{max} = k_2e_0$, $K_m = \frac{k_{-1}+k_2}{k_1}$. The result is unsurprising when compared to the single substrate rate equation of s because we have only replaced s with s^2 . We use (1.8d) to show that the change in product is equal to the negative change in substrate concentration. It is possible to construct a graph of this rate equation similarly to Figure 1.3. The difference between the two graphs is that we now produce a sigmoidal graph, where $\sqrt{K_m}$ is the concentration required for half of the maximal rate.

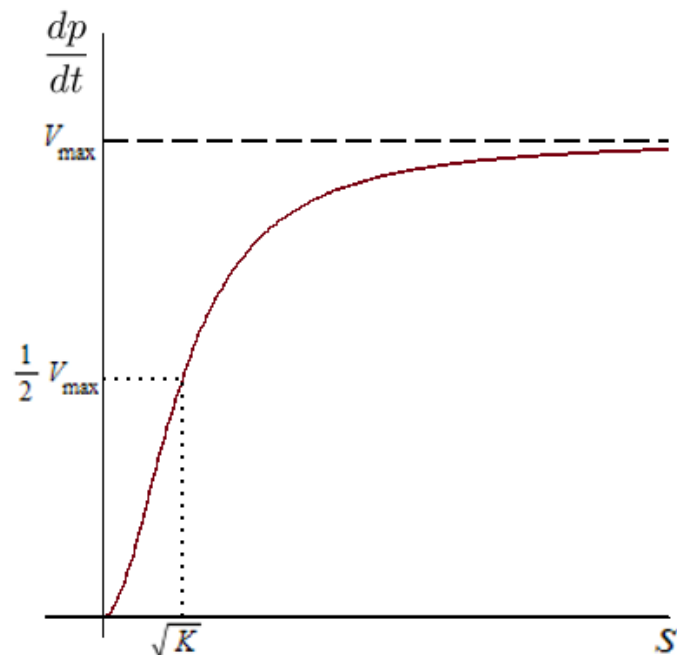


Figure 2.1: Graph of rate equation of reaction. Similar to Figure 1.2, yet the curve now has a point of inflexion. As substrate concentration s increases, the rate of product formation reaches V_{max} . When substrate concentration reaches a value $\sqrt{K_m}$, the rate of product formation is exactly $\frac{1}{2}V_{max}$.

2.2 Cooperative Reactions with Intermediate Steps

We discussed the reaction between two molecules of substrate reacting with one molecule of enzyme. However, the chances of three molecules colliding together are highly unlikely, so we look towards a different approach to the reaction. It is more realistic for one molecule of substrate to react with one molecule of enzyme. This will create one molecule of the (substrate-enzyme) complex, where another molecule of substrate will react with the complex. Products may be formed between these two steps, at rates k_2 and k_4 respectively. Another feature of this type of cooperative reaction, called the *allosteric effect* is when one substrate has bound with an enzyme at an active site. It can affect the reactivity to other active sites on the same enzyme. Such an enzyme is called an *allosteric enzyme*.

A great example of a cooperative reaction is the binding of oxygen to haemoglobin in the blood. The oxygen-carrying protein has four binding sites for oxygen to react. As one successfully reacts, the protein exhibits allosteric effects to which then further oxygen molecules can react at a faster, more successful rate. Going back to the two substrate case and putting it into perspective, the diagram below represents the two separate reactions:





Let lowercase letters denote the concentrations of the reactants in (22a,b)

$$s = [S], e = [E], c_1 = [E_1], c_2 = [E_2], p = [P] \quad (1.23)$$

As there are two new variables, c_1 and c_2 which replace c , we now have a system of five equations that we can interpret from the diagram of the reaction;

$$\frac{ds}{dt} = -k_1se + (k_{-1} - k_3s)c_1 + k_{-3}c_2 \quad (1.24a)$$

$$\frac{de}{dt} = -k_1se + (k_{-1} + k_2)c_1 \quad (1.24b)$$

$$\frac{dc_1}{dt} = k_1se = (k_{-1} + k_2 + k_3s)c_1 + (k_{-3} + k_4)c_2 \quad (1.24c)$$

$$\frac{dc_2}{dt} = k_3sc_1 - (k_{-3} + k_4)c_2 \quad (1.24d)$$

$$\frac{dp}{dt} = k_2c_1 + k_4c_2 \quad (1.24e)$$

with initial conditions: $s(0) = s_0, e(0) = e_0, c_1(0) = c_2(0) = p(0) = 0$.

The sum of the equations (1.24b) (1.24c) (1.24d) results in zero, hence with the conservation of enzymes we have;

$$\frac{de}{dt} + \frac{dc_1}{dt} + \frac{dc_2}{dt} = 0 \Rightarrow e + c_1 + c_2 = e_0 \quad (1.25)$$

with e_0 as a fixed constant. Using (1.25), we may eliminate e from equations (1.24a) (1.24b) (1.24c) (1.24d) (1.24e). As before, we nondimensionalise this system of equations. Let $\epsilon \ll 1$, so the dimensionless quantities chosen are

$$\begin{aligned} \tau = k_1e_0t, u(\tau) = \frac{s(t)}{s_0}, v_1(\tau) = \frac{c_1(t)}{e_0}, v_2(\tau) = \frac{c_2}{e_0} \\ a_1 = \frac{k_{-1}}{k_1s_0}, a_2 = \frac{k_2}{k_1s_0}, a_3 = \frac{k_3}{k_1}, a_4 = \frac{k_{-3}}{k_1s_0}, a_5 = \frac{k_4}{k_1s_0}, \epsilon = \frac{e_0}{s_0} \end{aligned} \quad (1.25)$$

with initial conditions;

$$u(0) = 1, v_1(0) = v_2(0) = 0$$

and so we obtain:

$$\frac{du}{d\tau} = -u + (u - a_3u + a_1)v_1 + (a_4 + u)v_2 \quad (1.26a)$$

$$\epsilon \frac{dv_1}{d\tau} = u - (u + a_3u + a_1 + a_2)v_1 + (a_4 + a_5 - u)v_2 \quad (1.26b)$$

$$\epsilon \frac{dv_2}{d\tau} = a_3uv_1 - (a_4 + a_5)v_2 \quad (1.26c)$$

Using the quasi steady state assumption and the initial conditions, it will lead us towards the rate equation. Let $\epsilon \ll 1$, which implies that both LHS of (1.26b)(1.26c) are equal to zero hence algebraic, so can be solved to obtain v_1 and v_2 in terms of u .

$$v_2 = \frac{a_3uv_1}{a_4 + a_5} \quad (1.27a)$$

By substitution into (1.26b), we obtain:

$$v_1 = \frac{u}{u + a_1 + a_2 + a_3u^2(a_4 + a_5)^{-1}} \quad (1.27b)$$

Substituting into (1.26a) and after many cancellations:

$$\begin{aligned} \frac{du}{d\tau} &= -u \frac{a_2 + a_3a_5u(a_4 + a_5)^{-1}}{a_1 + a_2 + u + a_3u^2(a_4 + a_5)^{-1}} \\ &= -r(u) < 0 \end{aligned} \quad (1.28)$$

In dimensionless terms, using (1.25), the rate equation for the reaction, denoted by $R_0(s_0)$ becomes;

$$R_0(s) = \left. \frac{ds}{dt} \right|_{t=0} = e_0s \frac{k_2K'_m + k_4s}{K_mK'_m + K'_ms + s^2} \quad (1.29)$$

$$K_m = \frac{k_2 + k_{-1}}{k_1}, K'_m = \frac{k_4 + k_{-3}}{k_3}$$

where K_m and K'_m are the Michaelis constants, which are equivalent to the Michaelis constant in (1.8b).

This rate can look very similar to (1.21), and it is very possible to conclude which expressions can be ignored to link the two together. Referring back to the mechanism,

if a molecule of s combines with an enzyme and due to the allosteric effect the second molecule, c_2 complexes more readily so we are able to assume that the rate of which this specific reaction occurs, k_3 , is very fast. Due to this, we neglect the intermediate complex c_1 as it is short lived. Another assumption to make is that in the numerator, the term linear in s is removed if $k_2 = 0$, which occurs if products are not formed during the intermediate step. Combining both, this leads straight the model given by (1.21). We see that they are very similar and both graphs show a Hills plot. When cooperative behaviour is shown in enzymatic reactions, Hill plots are generally formed as most rate equations for such reactions are of the form;

$$R_0(s) = \frac{Qs^n}{K_m + s^n} \quad (1.30)$$

where $n > 0$ is generally an integer, and it labelled the *Hill equation*.

To create a *Hill plot*, a graph of $\ln[\frac{R_0}{Q-R_0}]$ against $\ln s_0$ is required, and so by solving (1.30) for s^n we obtain:

$$s^n = \frac{R_0 K_m}{Q - R_0} \Rightarrow n \ln s = \ln K_m + \ln \frac{R_0}{Q - R_0} \quad (1.31)$$

The gradient of a Hill plot will give the value of n and will stay constant provided the Hill equation describes the rate of reaction in question.

Chapter 3

Positive and Negative Feedback Systems

We know the importance of enzymatic reactions, but we must also know the importance of regulating them. Many products formed in such reactions act as an allosteric activator, or inhibitor (positive or negative) for the reaction which forms an intermediate product. Thus, the reaction is aptly named as a *feedback loop*. It is important to understand how to obtain a stable steady state for such circuits as both proteins may become depleted or over produced over time. For example, let us have a system of two proteins A and B.

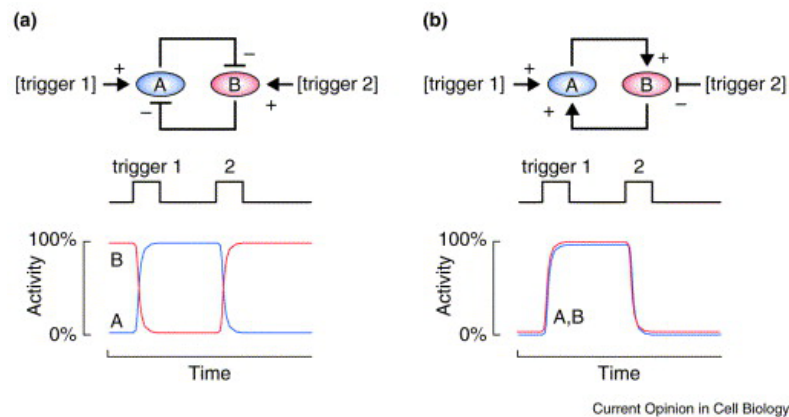


Figure 3.1: (a): A double-negative feedback loop. From the circuit, we see that Protein A acts as an inhibitor in the reaction to produce protein B. Protein B also acts as an inhibitor, but for the production of protein A. It is possible to have a stable steady state for A on and B off, or A off and B on. However it is impossible in situations with both A and B on, or both off. It is possible however, for trigger stimuli to affect the feedback loop such as to switch the steady state between “A-on, B-off” and “A-off, B-on”. (b): A positive feedback loop. Protein A activates protein B, and B activates A in this circuit. It is possible to achieve a stable steady state if both A and B are off, or both on. However, we cannot achieve this with one of A or B on whilst the other is off. These two circuits can produce a self-sustaining pattern of protein activity. Figure from text [7].

Mathematically modelling such biological systems gives a greater insight into a reaction. If succeeding in replicating a reaction, it shows that all interactions within have been identified, whereas a negative result indicates a fault with qualitatively understanding the mechanism in question. We may also find out which parameters manipulate the outcome of results. For example, showing how much concentration of a molecule is required for production of another, with increased presence of an inhibitor. It is possible to describe the dynamics of a biological system with a simple ODE model, when stochastic effects are considered negligible and are useful for when biological oscillators and switches are used.

3.1 Yeast Glycolytic Oscillations

A great example of a two variable system to inspect is the Bier et al. model of Yeast glycolytic oscillations. We have a concentration of glucose, $[G]$ outside of the yeast cell, entering through at a rate v_{in} , to which it then converts into $[ATP]$ at a rate k_1 by a process called *glycolysis*. While glycolysis converts ATP from glucose, it also requires ATP to initiate the reaction (hence the dashed-line on 3.2). ATP then also is consumed and converted into ADP, with concentration $[ADP]$ at a rate k_p . Whilst ATP is increased, there is an increase in ADP and also an increase in the formation of ATP from G_{in} . Assumptions are made to simplify the model, such as that there are many ATPases involved in the mechanism, however we can combine all together, and so we just have one whole concentration of ATP. Another assumption is that glycolysis is represented through a different amount of enzymes, and by assuming all other intermediate steps occur quickly apart from the rate limiting step, phosphofructokinase, we can consider the rate constant to just be k_1 .

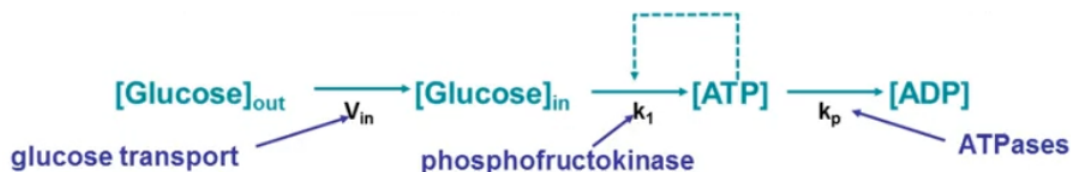


Figure 3.2: Diagram depicting glycolysis and how ATP is used to catalyse the reaction that produces ATP. Figure from [5]

We are interested here in the rate of which ATP changes, and the rate of which glucose inside the cell changes. Let us consider a system of ODEs for the model above.

We shall label both derivatives as f and h respectively,

$$\frac{dA}{dt} = 2k_1GA - \frac{k_pA}{A + K_m} = f \quad (3.1a)$$

$$\frac{dG}{dt} = v_{in} - k_1GA = h \quad (3.1b)$$

where $[ATP] = A$ and $[G] = G$. Looking closely at (3.1a) we see that the positive term represents the increase of $[ATP]$ from the conversion of $[G]$, and the negative term is the decrease of $[ATP]$ through conversion into $[ADP]$. Also note that the negative term includes a michaelis constant, K_m . For the model above, there are 3 default parameters:

$$v_{in} = 0.36, k_1 = 0.02, k_p = 6 \quad (3.1c)$$

However, when we change the values of other parameter, K_m , we obtain some interesting results. If we are to plot both $[ATP]$ and $[G]$ against time, using the default parameters, we will consider two cases, notably when $K_m = 13$ and $K_m = 20$.

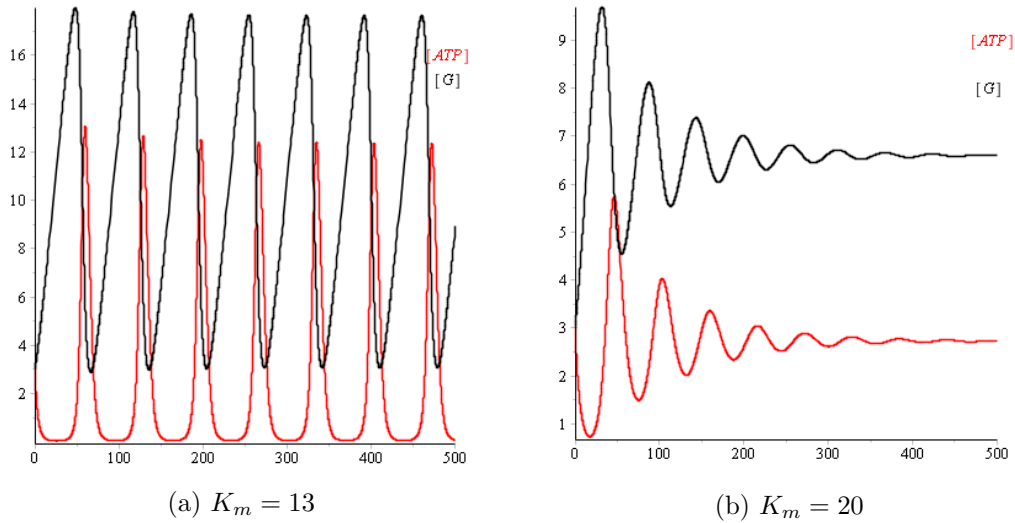


Figure 3.3: Plots of concentration of Glucose (black) and ATP (red) against time. (a) Showing oscillatory behaviour, When ATP increases, Glucose is decreased, and vice versa. (b) Showing damped oscillations, that over time both ATP and G each converge to a steady state value.

We can see in Figure 3.3 how that for $K_m = 13$, oscillations are shown, whereas for $K_m = 20$, damped oscillations are shown. However, this does not give a clear understanding of the qualitatively different behaviour between the two cases. By introducing phase plane techniques, we are able to analyse our 2-dimensional example above for

both values of K_m . This involves plotting a graph of $[G]$ against $[ATP]$, but first we must conclude where there are fixed points if any and determine their stability.

This is possible by determining the points at which both derivatives, (3.1a) and (3.1b) are equal to zero and also by using our set of default parameters and for the different values of $K_m = 13$ and $K_m = 20$. Such fixed points, A^* and G^* can be calculated using the selected parameter values:

$$(A^*, G^*) = \left(\frac{2v_{in}K_m}{k_p - 2v_{in}}, \frac{k_p - 2v_{in}}{2k_1K_m} \right)$$

$$\Rightarrow (A^*, G^*)_{(K_m=13)} = \left(\frac{39}{22}, \frac{132}{12} \right) \quad (3.2a)$$

$$(A^*, G^*)_{(K_m=20)} = \left(\frac{30}{11}, \frac{33}{5} \right) \quad (3.2b)$$

What is unclear at this moment is whether the fixed point is stable or unstable, which can be calculated numerically. This can be determined in a more mathematical rigorous approach by using a Jacobian matrix and analysing the eigenvalues produced at that specific fixed point. Let us consider our two derivatives f and h . By computing the Jacobian matrix, we obtain:

$$J = \begin{bmatrix} \frac{\partial f}{\partial A} & \frac{\partial f}{\partial G} \\ \frac{\partial h}{\partial A} & \frac{\partial h}{\partial G} \end{bmatrix} = \begin{bmatrix} 2k_1G + \frac{-k_p(A+K_m)+k_pA}{(A+K_m)^2} & 2k_1A \\ -k_1G & -k_1A \end{bmatrix} \quad (3.3a)$$

Now by inputting our fixed points, we obtain:

$$J_{(K_m=13)} = \begin{bmatrix} 0.0487384614 & 0.07090909092 \\ -0.2030769230 & -0.03545454546 \end{bmatrix} \quad (3.3b)$$

$$J_{(K_m=20)} = \begin{bmatrix} 0.0316800001 & 0.1090909091 \\ -0.1320000000 & -0.5454545454 \end{bmatrix} \quad (3.3c)$$

By using a software such as maple, we are able to find the eigenvalues for both cases of K_m values and evaluate them to determine the stability of the fixed points (3.2a) and (3.2b). The eigenvalues that were found are the following:

$$E_1 = 0.664195797000000 + 0.112373859930719i$$

$$E_2 = 0.664195797000000 - 0.112373859930719i \quad (3.4a)$$

for the fixed point (3.2a) and,

$$E_3 = -0.114327272200000 + 0.111987913384576i$$

$$E_4 = -0.114327272200000 - 0.111987913384576i \quad (3.4b)$$

for the fixed point (3.2b).

As we can see, both sets of eigenvalues are complex conjugates. Using our understanding of stability theory, we may use the following statement to determine the stability of the fixed points:

Definition 3.1.1. Stability of a Steady State: In a continuous model, a steady state will be stable provided that the eigenvalues determined from the Jacobian matrix are both negative (if real) or have negative real parts (if complex). That is,

$$Re(\lambda_i) < 0 \text{ for all } i.$$

For (3.4a), the real parts of both eigenvalues are positive, and so does not fit the criteria of a stable point hence is unstable. However for (3.4b), both real parts of the eigenvalues are negative when $K_m = 20$, which fits with our criteria of a stable point. There are many type of stable points however, and so it may prove useful to determine which of these it is. Using the following diagram, we can assort our point into their own individual type.

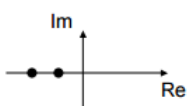



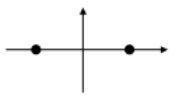
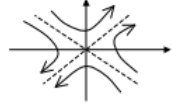
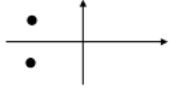
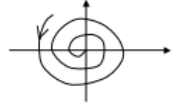
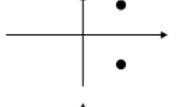
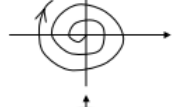


Eigen value	T	Δ	$T^2 - 4\Delta$	Steady state	Phase plot
	$T < 0$	$\Delta > 0$	$T^2 - 4\Delta > 0$	stable node	
	$T > 0$	$\Delta > 0$	$T^2 - 4\Delta > 0$	unstable node	
	$T > 0$ ou $T < 0$	$\Delta < 0$	$T^2 - 4\Delta > 0$	saddle (unstable)	
	$T < 0$	$\Delta > 0$	$T^2 - 4\Delta < 0$	stable focus	
	$T > 0$	$\Delta > 0$	$T^2 - 4\Delta < 0$	unstable focus	
	$T = 0$	$\Delta > 0$	$T^2 - 4\Delta < 0$	center (marginal stability)	

Figure 3.4: The steady state value can be assigned to many types, determined by their corresponding eigenvalues. Where T is the Trace of the Jacobian matrix, Δ is the determinant and $T^2 - 4\Delta$ is the discriminant.

Comparing to the diagram, our steady state value of $K_m = 20$ corresponds to a “stable focus”, as it has complex conjugate parts as well as both real parts being

negative. Whereas, for $K_m = 13$, we have an “unstable focus”. Acknowledging the results from our stability analysis is a vital part in the overall picture, to which now we are able to construct a phase portrait. This is to show that with small perturbations from the system, it will always tend to the limit cycle and stable fixed point for our respective K_m values. It is also useful to plot a phase portrait as we are able to see in which direction the system is moving, governed by the two equations (3.1a) and (3.1b), at which any point is determined by a vector defined by the derivatives with respect to time.

We are able to go a step further and determine which regions the direction changes by plotting *nullclines*, of G against ATP . These nullclines in question are the set of all points at which (3.1a) and (3.1b) are individually equal to zero. Considering both equations, by inspection it is easier to make G the subject of both equations, due to the saturating term in (3.1a). Plotting both curves against each other will contrast to the fixed points within the system, which will be the point at which both curves intersect.

$$\begin{aligned} \frac{dA}{dt} &= 2k_1GA - \frac{k_pA}{A + K_m} = f = 0 \\ \Rightarrow G &= \frac{k_p}{2k_1(A + K_m)} \end{aligned} \quad (3.5a)$$

$$\begin{aligned} \frac{dG}{dt} &= v_{in} - k_1GA = h = 0 \\ \Rightarrow G &= \frac{v_{in}}{k_1A} \end{aligned} \quad (3.5b)$$

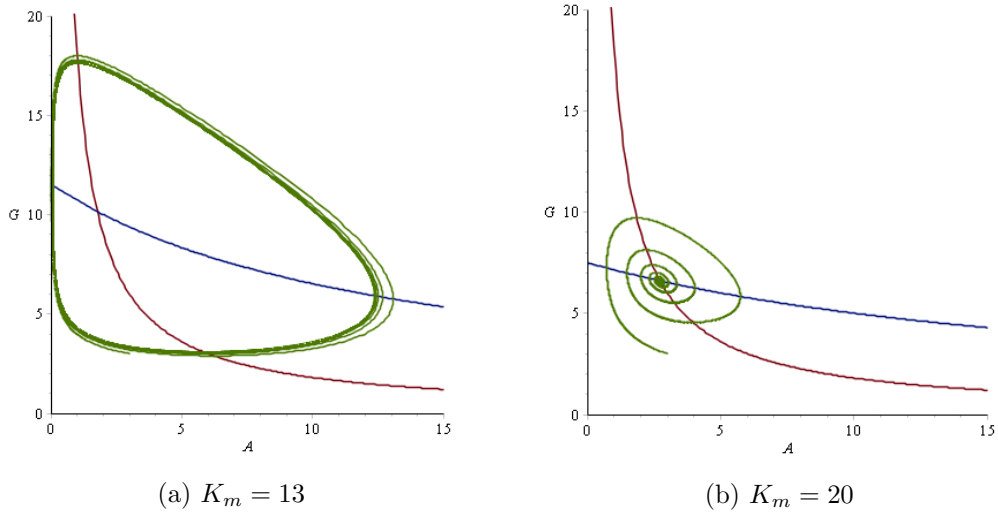


Figure 3.5: Phase portraits of the system (3.1a-b) including G (blue) and ATP (red) nullclines with concentration of glucose, G against concentration of ATP , A for both values of $K_m = 13$ and $K_m = 20$. (a) Stable limit cycle. (b) Spiral converging towards stable fixed point.

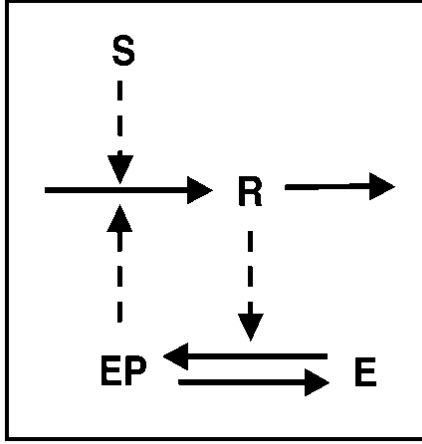
Consider now the default parameters and both values of K_m , the plots of which are shown above. As seen from Figure 3.5, the nullclines for both (a) and (b) intersect at the respective fixed point values (3.2a) and (3.2b). The ATP nullcline (red) for both cases does not differ as it does not depend on K_m . Notice that for value of $K_m = 13$, we have a limit cycle which shows the change of oscillatory behaviour for both [G] and [ATP]. Also for $K_m = 20$, we see a converging spiral shape, showing the damped oscillations which eventually converge to a fixed point, which we proved to be stable. Also from Figure 3.5, we see that for $K_m = 13$ the direction of the stable limit cycle oscillates in a clockwise motion. For $K_m = 20$, the direction of the spiral converges to the stable fixed point in clockwise motion. We are able to see this from the trajectory from initial conditions for each value of K_m .

For $K_m = 13$, the reason for obtaining a stable limit cycle is due to the Poincaré-Bendixson Theorem, that as time tends towards infinity, the trajectory of the system matches the trajectory of the stable limit cycle as time tends towards infinity (p.327-330) [1]. The limit cycle may correspond to the idea that the system overshoots the production of Glucose and ATP, and tries to balance the system, ultimately ending with this oscillatory behaviour. However with $K_m = 20$, we see that the system successfully balances itself to the stable steady state values for Glucose and ATP.

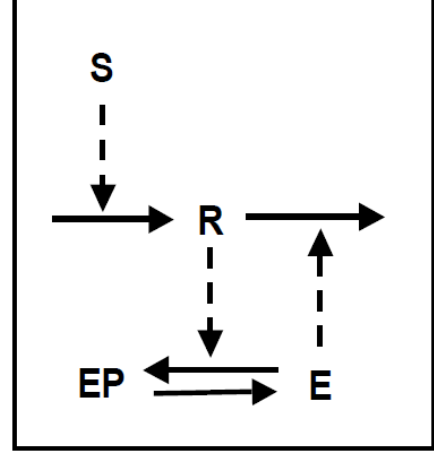
3.2 Bistability: Mutual Activation and Mutual Inhibition

A bistable system may be defined as a system that can switch between two alternative stable steady-states. Such bistability, under certain circumstances, will convert a transient trigger stimulus into an irreversible response. The qualities required for bistability include positive feedback, double-negative feedback, autocatalysis, or the equivalent. However, bistability of a system is not guaranteed by such feedback. A bistable system must also mathematically include three fixed points, two of which need to be stable and one unstable. Both sides of such a feedback loop must be properly balanced for the circuit to be bistable; if either is too strong or too weak, the circuit will be monostable rather than bistable. Thus, feedback is required for bistability, but does not guarantee it.

Bistable circuits show a certain degree of hysteresis, the time-based dependence of a circuit's output on current and past inputs such as, if it began in its off or on state. However, bistability does not guarantee irreversibility due to hysteresis, meaning it shows difficulty in switching from one state to the other, rather than to maintain the system in its flipped state. This irreversibility is shown when we have a sufficiently strong feedback system, and will stay in its flipped state even after the stimulus trigger is removed.



(a) Mutual activation



(b) Mutual inhibition

Figure 3.6: (a) Model of how a stimulus, S triggers a response, R which catalyses the phosphorylation of enzyme, E . This then catalyses the synthesis of R , so that as R increases, there is an increase in phosphorylation of E . (b) Model of how a stimulus, S triggers a response, R which catalyses the phosphorylation of enzyme, E to become E_p . This then leads to the degradation of R . Figure from [4].

By understanding what it means mathematically for a circuit to be bistable, we will be able to conclude which parameters need to be set at specific levels of concentrations. Looking further into two examples, mutual activation and mutual inhibition, we are able to use the same type of analysis used for the Bier et al. model mentioned in the last section to determine such bistability. Referring to an example of mutual activation from [4], as seen in figure 3.3 above, we are able to model the reaction as a system of ODEs. Note that,

$$[E]_T - [E] = [E]_P \quad (3.5)$$

where E_T is the concentration of enzyme total, E the total concentration of de-phosphorylated enzyme and E_P the total concentration of phosphorylated enzyme. By rearranging to reduce the amount of variables then substituting into our ODE system, we obtain;

$$\frac{dR}{dt} = k_{1R}(E_T - E) + k_{1R}S - k_{2R}R = f_1 \quad (3.6a)$$

$$\frac{dE}{dt} = -k_{2E} \frac{E}{E + K_{m2E}} + k_{1E} \frac{E_T - E}{E_T - E + K_{m1E}} = h_1 \quad (3.6b)$$

where k_{1R} is the rate of synthesis of R , k_{2R} the rate of conversion of R , k_{1E} the rate of phosphorylation of E , k_{2E} the rate of de-phosphorylation of E_P , and K_{m1E} , K_{m2E}

are the michaelis constants of the reaction. As both mutual activation and mutual inhibition examples are analysed using the same method of stability analysis, we will only delve further into bistability analysis for the mutual inhibition model.

Another very similar example from [4] is that of mutual inhibition, the model of which is shown as an ODE system below:

$$\frac{dR}{dt} = k_{0R} + k_{1R}S - (k_{2R} + k_{3R}E)R = f_2 \quad (3.7a)$$

$$\frac{dE}{dt} = -k_{2E}R \frac{E}{E + K_{m2E}} + k_{1E} \frac{E_T - E}{E_T - E + K_{m1E}} = h_2 \quad (3.7b)$$

The set parameter values to make numerical calculations and graphs are the following: $k_{0R} = 0$, $k_{1R} = 0.05$, $k_{2R} = 0.1$, $k_{3R} = 0.5$, $k_{1E} = 1$, $k_{2E} = 0.2$, $K_{1mE} = 0.05$, $K_{m2E} = 0.05$, $E_T = 1$. By plotting nullclines we are able to conclude where three intersections will occur, which will be the three fixed points required. This can be achieved by setting the RHS of both (3.7a) and (3.7b) equal to zero and rearranging for R as it is easier to obtain than E .

$$R = \frac{k_{0R} + k_{1R}S}{k_{2R} + k_{3R}E} \quad (3.8a)$$

$$R = \frac{\frac{k_{1E}(E_T - E)}{(E_T - E) + K_{m1E}}}{\frac{k_{2E}E}{E + K_{m2E}}} \quad (3.8b)$$

By inspection of Figure 3.7, we see that for $S = 10$, there is only one intersection between the null clines. The level of stimulus is too high for bistability, and so we obtain a monostable scenario. Also, for $S = 2$, there is one intersection, so to conclude for both values of S stated, it is impossible to obtain bistability. However, there are clearly three intersection between the null clines for value $S = 6$, and hence we have three fixed points which is our mathematical basis of bistability.

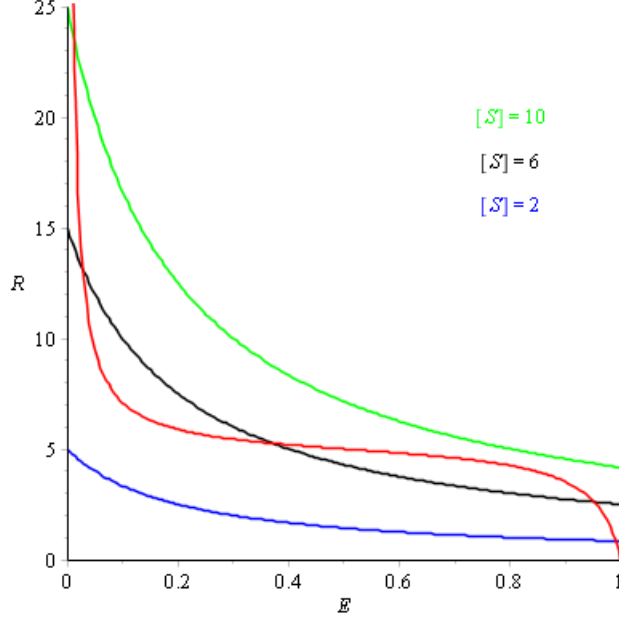


Figure 3.7: Plot of concentration of response, R against concentration of enzyme, E . For value of $S = 6$, there are three equilibria points, indicating a basis for bistability.

By constructing a Jacobian matrix at these fixed points, we are able to evaluate and determine the stability of these three fixed points by analysing the respective eigenvalues. The equilibria of this system are found when (3.7a) and (3.7b) are both equal to zero. By inputting the given parameters and by using a mathematical software such as maple, we are able to numerically find such fixed points. They are as follows:

$$(R^*, E^*)_1 = (13.13668170, 0.2836817308) \quad (3.9a)$$

$$(R^*, E^*)_2 = (5.256745294, 0.3706953318) \quad (3.9b)$$

$$(R^*, E^*)_3 = (2.606573006, 0.9509364951) \quad (3.9c)$$

$$J(f_2, h_2) = \begin{bmatrix} \frac{\partial f_2}{\partial E} & \frac{\partial f_2}{\partial R} \\ \frac{\partial h_2}{\partial E} & \frac{\partial h_2}{\partial R} \end{bmatrix} =$$

$$= \begin{bmatrix} -k_2ER \left(\frac{1}{E+K_{m2E}} - \frac{E}{(E+K_{m2E})^2} \right) + k_1E \left(\frac{(E_T-E)}{(E_T-E+K_{m1E})^2} - \frac{1}{(E_T-E+K_{m1E})} \right) & -k_3R \\ -k_2E \left(\frac{E}{E+K_{m2E}} \right) & -(k_2R + k_3RE) \end{bmatrix} \quad (3.10)$$

Similarly to our previous model with oscillatory behaviour, we can analyse the stability of the jacobian by determining the eigenvalues at each individual Jacobian matrix, corresponding to the fixed points found earlier. For $(R^*, E^*)_i$ with $i = 1, 2, 3$, the corresponding Jacobian matrices with their eigenvalues are the following:

$$J_1 = \begin{bmatrix} -21.43768081 & -0.07239717852 \\ -6.568340850 & -0.1141840865 \end{bmatrix}$$

$$\lambda_1 = -21.4599582566415$$

$$\lambda_2 = -0.919066398584615 \quad (3.11a)$$

$$J_2 = \begin{bmatrix} -0.4053701321 & -0.1762298289 \\ -2.628372647 & -0.2853476659 \end{bmatrix}$$

$$\lambda_3 = -1.02858580857282$$

$$\lambda_4 = 0.337868010572825 \quad (3.11b)$$

$$J_3 = \begin{bmatrix} -5.120998640 & -0.1900093562 \\ -1.303286503 & -0.5754682476 \end{bmatrix}$$

$$\lambda_5 = -5.17484004278428$$

$$\lambda_6 = -0.521626844815719. \quad (3.11c)$$

It is clear that every eigenvalue has no complex part, so there is no rotation. Using the stability criteria Definition 3.1.1, we see that for (3.11a) and (3.11c) both eigenvalues are negative, hence we have two stable points corresponding to our fixed points (3.9a) and (3.9c). In addition, for (3.11b) we see that one of the eigenvalues is positive and so this corresponds to an unstable fixed point for (3.9b).

By determining that the system has two stable fixed points, separated by an unstable fixed point in between, we can now confirm that the system shows bistability, a useful property in biological systems. An example of such is to regulate the concentrations of proteins within a system.

Possibly all biochemical reactions involved in cell signalling are reversible, however, many biological transitions are irreversible. For both cases (mutual activation or inhibition), positive feedback may create a discontinuous switch. This means that the cellular response changes abruptly and irreversibly as signal concentration crosses a threshold value of S .

Let us plot a bifurcation plot of the steady state value of R against the stimulus concentration, S for both mutual activation and mutual inhibition examples.

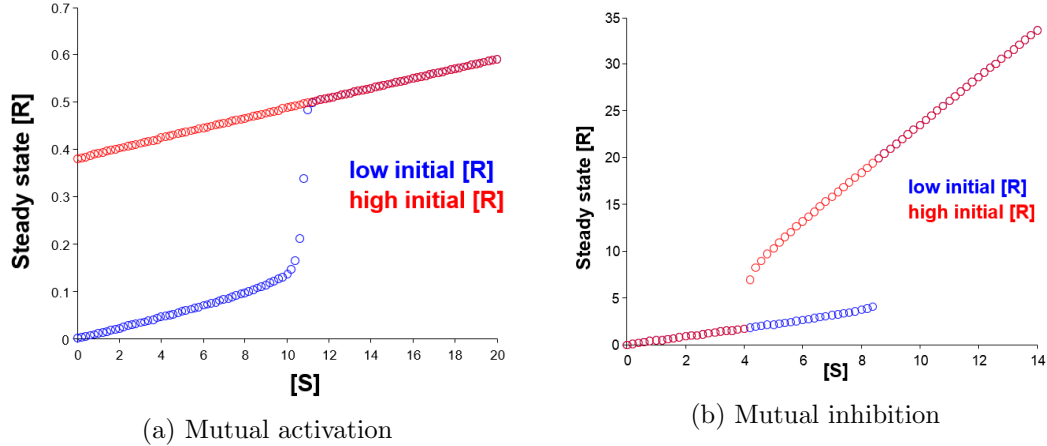


Figure 3.8: Bifurcation plots showing *hysteresis* for steady state values, R against stimulus concentration S . (a): Example showing irreversibility, how after stimulus is increased passed a critical value, concentration of R will remain high even after removal of stimulus. In other words, activity of R will remain in the 'on' state.(b): Bistable switch, where R will go back to the 'off' state after removal of sufficient S . Figures from [6].

Inspecting Figure 3.8 for a low initial R value, as the stimulus concentration S increases when it surpasses a threshold value of S the response value increases abruptly towards a higher value. After the removal of S , the response stays at a high value, implying the *irreversible* quality of the system. For S values between $S = 0$ and $S \approx 11$, the system is bistable as it has two steady state values for S . The steady state response is an indicator of the behaviour of the system as a function of the stimulus. At $S_{crit} \approx 11$, the behaviour of the system changes irreversibly from low response to high response (or vice versa). Such points of qualitative change in the behaviour of a nonlinear system are called bifurcation points.

Considering also Figure 3.8B, for a low initial R value, as S increases past a value of $S \approx 9$, the response value increases abruptly towards a higher value. This also occurs for a higher initial R value, but at a threshold value of $S \approx 4$. However the difference between this example is that after removal of sufficient stimulus S , the system will return back towards a lower R value. For values of S between $S \approx 4$ and $S \approx 9$ the system is bistable as it has two stable steady state response values, which are separated by an unstable steady state. This 'toggle switch' (two-way discontinuous switch) example is often referred as *hysteresis*.

Discontinuous responses appear to be one of the two switches: the one-way switch (mutual activation example), and the toggle switch (mutual inhibition example). One-way switches presumably are a key feature of developmental processes characterized by the being unable to revert back during or after a developmental part of the process. Frog oocyte maturation in response to progesterone is an example of such, as is Apoptosis [4].

Chapter 4

The Sonic Hedgehog (Shh) Signalling System

4.1 Introduction to the Shh Pathway

Cells go through rigorous transformations via complex regulatory signals during developmental stages of life. Without the ability to correctly interpret such signals, they cannot implement necessary functional decisions. Such information processing mechanisms are important, to interpret extracellular information into intracellular decisions. The fate of such cells are determined by the exposure to a concentration of an external signal at specific key intermediate steps, to which they commit to a decision by switching between two alternate behaviours in an all-or-none fashion. Such an example is Apoptosis, the decision for a cell to die instead of surviving. It isn't possible for a cell to forty percent commit to die, hence the all-or-none switch behaviour. We theoretically can find more information concerning cellular processing by analysing the signalling mechanisms of such a morphogen (a substance that causes an organism to develop its shape) named *Sonic hedgehog*.

In vertebrates, one of the three mammalian homologs of the *Hedgehog family*, Sonic hedgehog (Shh), is a signaling factor that regulates cell functionality and their fate in many biological systems. It has an important role to play in development by determining the pattern of spinal cord and limb bud tissue differentiation, and controls midbrain and ventral forebrain neuronal differentiation. Among other functions, it is responsible for feathers forming in correct places on chicks, and positioning human pinkies to be our most posterior digits [9]. By forming a concentration gradient, Shh can pattern tissue during development, seen in the neural tube and spinal cord, to which cells are able to sense the position of themselves within the concentration gradient. They then go on to transform into distinct cell phenotypes (observable characteristics or traits), determined by this concentration gradient. Remarkably, Shh is capable of signalling up to 20 cell diameters away from its source. It is key to note that Shh has the ability to switch a cell between its alternate functional state at specific threshold concentrations

[11]. By quantitatively analysing the Shh gene regulatory network, an insight into its properties that allow it to function as a switch, and to malfunction during disease is found.

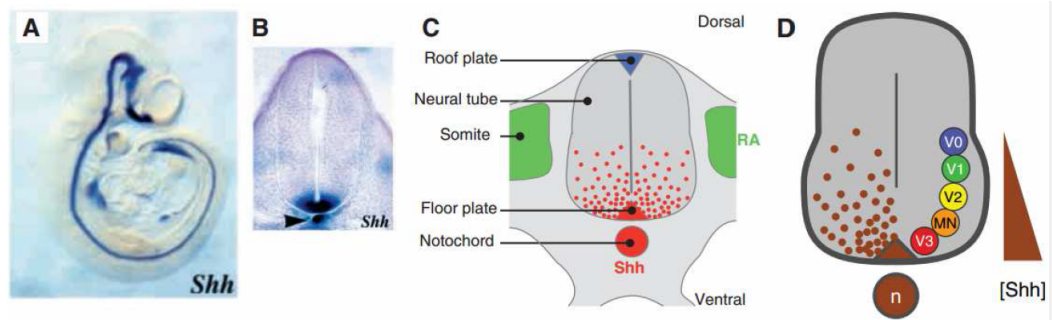


Figure 4.1: Image (A) of Shh concentration in the lumbar region of the spinal cord of the embryo in (B), showing the notochord and floor plate (darker areas). Diagram (C) depicting how Shh concentration (red) from the notochord and floor plate spreads through the ventral neural tube, generating a ventral to dorsal concentration-gradient. Diagram (D) showing the different neural progenitor domains. Labels of V0 to V3 are four different classes of ventral interneurons, whereas MN indicates motor neurons.

The neural tube (precursor to development of the spinal cord and brain), formed from the neural plate hosts many different cell phenotypes which are initially, mostly identical. Before they develop into these cell phenotypes, they react to their position along the rostro-caudal and dorsoventral axis (tail end of Figure C) within the neural tube from the surrounding concentration of Shh. Shh concentration is secreted from the notochord and floor plate, which then spreads through the ventral neural tube causing this concentration-gradient mentioned earlier. This is the basis of the formation of a variety of neurons and glial cells (cells that hold together and protect neurons), that form a functional nervous system. Neuronal subtype specification is determined by the concentration of Shh, which establish distinct levels of signalling in the responsive cells. This regulates target genes and causes the different groups of neurons to express different types of transcription factors. (e.g *Nkx2.2*, *Olig2*). The subdividing of the ventral neuroepithelium into five different neural progenitor domains, which each generate distinct neuronal subtypes are caused by these transcriptional factors, as seen in figure 4.1D.

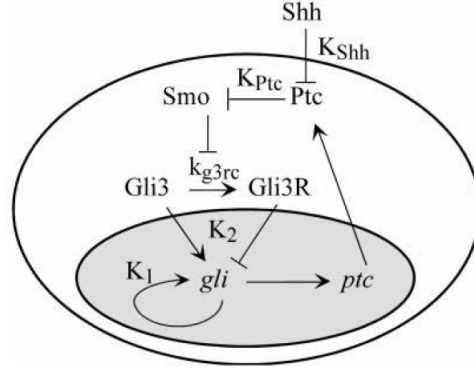


Figure 4.2: Schematic diagram of the Shh signaling system. Shh binds to Ptc, disabling the Ptc repression on activity of Smo. Smo signaling inhibits the conversion of the transcription factor factor Gli3 from an activator to a repressor. The accumulation of Gli3 then activates the genes *gli* and *ptc*. Gli1 binds and activates its own promoter, as well as the signal repressor Ptc [10].

This model for tissue patterning in Figure 4.2 was determined by Lai et al. [10]. Interacting with the transmembrane receptor Patched (Ptc), Shh is then able to transduce it's signal into the cells themselves. This allows the signalling of the transmembrane protein Smoothened (Smo), to go forward and transduce a signal by activating members of the Gli family of transcription factors. This results in the depletion in Shh concentration from the extracellular space. However in the absense of Shh, Ptc represses the signalling activity of Smo, which causes Gli3 to be cleaved and generates a transcription factor Gli3R which represses the activity of Shh targets. With the activation of Smo, the rate of Gli3 cleavage is reduced and the resulting accumulation of Gli3 then activates the transcription of a number of Shh targets (*ptc*, *shh*, *gli1* and *gli2*), while *gli3* is also repressed due to Shh signalling. Gli1 and Gli2 act as transcriptional activators (which are lumped together to form the term Gli) and bind to the same sites as Gli3, inducing positive feedback on their own expression and activate targets which mediate the downstream cell regulatory effects of Shh signalling. However, the Shh system also shows signs of negative feedback due to Gli transcriptionally activating the signal repressor Ptc.

4.2 Shh Mathematical Model

Dynamic modelling of such a complex signalling and gene regulatory network can substantially increase our understanding of the model in ways in which may not be discovered from a biological point of view. A simplified version of the system can be represented by the set of four differential equations, shown below:

$$\frac{dGli}{dt} = v_{max,G}Promoter + r_{bas,G}Basal - k_{deg}Gli \quad (4.1a)$$

$$\frac{dGli3}{dt} = \frac{r_{g3b}}{Ptc} - Gli3 \left[k_{deg} + \frac{k_{g3rc}}{K_{g3rc} + Signal} \right] \quad (4.1b)$$

$$\frac{dGli3R}{dt} = Gli3 \left[\frac{k_{g3rc}}{K_{g3rc} + Signal} \right] - k_{deg}Gli3R \quad (4.1c)$$

$$\frac{dPtc}{dt} = v_{max,P}Promoter + r_{bas,P}Basal - k_{deg,P}Ptc \quad (4.1d)$$

where

$$Signal = \frac{1 + \frac{Shh}{K_{Shh}}}{1 + \frac{\left(K_{Shh} + \frac{Ptc}{K_{Ptc}} \right)}{Shh}} \quad (4.1e)$$

with the promoter and basal terms defined below

$$Promoter = \frac{A_1(B_1 + C_1)}{D_1 + E_1 + F_1} \quad (4.1f)$$

where

$$\begin{aligned} A_1 &= (Gli3K_1 + GliK_2) \\ B_1 &= 3e^2K_1^2K_2^2 + 3ceK_1K_2(Gli3K_1 + GliK_2 + 2eGli3RK_1r) \\ C_1 &= c^2(Gli3^2K_1^2 + Gli^2K_2^2 + 3eGliGli3rK_1K_2r + 3e^2Gli3R^2K_1^2r^2 \\ &\quad + Gli3K_1(2GliK_2 + 3eGli3RK_1r)) \\ D_1 &= 3cK_1K_2(Gli3K_1 + Gli3RK_2 + GliK_2)^2 \\ E_1 &= c^2(Gli3K_1 + Gli3RK_1 + GliK_2)^3 \\ F_1 &= K_1^2K_2^2(3Gli3K_1 + 3Gli3RK_1 + (3Gli + K_1)K_2) \end{aligned}$$

and

$$Basal = \frac{A_2 + B_2 + C_2}{D_2 + E_2 + F_2} \quad (4.1e)$$

where

$$\begin{aligned} A_2 &= 3cK_1K_2(Gli3K_1 + GliK_2 + Gli3RK_1r)^2 \\ B_2 &= c^2(Gli3K_1 + GliK_2 + Gli3RK_1r)^3 \\ C_2 &= K_12K_2^2(3Gli3K_1 + 3GliK_2 \\ D_2 &= 3cK_1K_2(Gli3K_1 + Gli3RK_1 + GliK_2)^2 \\ E_2 &= c^2(Gli3K_1 + Gli3RK_1 + GliK_2)^3 \\ F_2 &= K_1^2K_2^2(3Gli3K_1 + 3Gli3RK_1 + (3Gli + K_1)K_2) \end{aligned}$$

The derivation of both promoter and basal equation can be found in the supplementary data of [10], where they assume quasi steady state binding between promoter and transcription factors. In addition, they allowed for the possibility of cooperative protein binding to the promoter, such that promoter with one or more factors bound had an increased affinity for the next factor, the binding cooperativity factor c (allosteric effect, mentioned in chapter 2). Sigmoidal graphs can be produced of both *Promoter* and *Basal* against *Gli* (with $Gli3 = 0$) at varied concentrations of the inhibitor, *Gli3R*

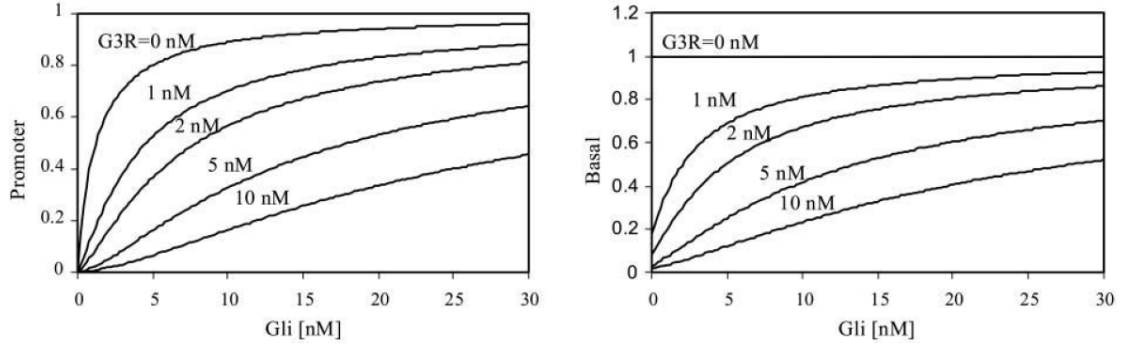


Figure 4.3: The functions are ratios of polynomials, which vary between values of 0 and 1, describing the inducible and basal activities of the *gli* and *ptc* promoters varying with the concentrations of the three transcription factors that bind them - *Gli3*, *Gli3R* and *Gli*. Note that *G3R* refers to *Gli3R* concentration. Figures from [10]

Referring to (4.1a), we see that there are two promoting terms to the equation, followed by the degradation of *Gli* at a rate of k_{deg} . The promoting term, $v_{max,G}Promoter$, is due to the transcriptional activation of the gene *Gli*, whereas $r_{bas,G}Basal$ is due to the basic rate of transcriptional activation of *Gli*. (4.1b) has an increasing term that is inversely proportional to the level of Ptc concentration which can be explained by the resulting activation of *Smo* reducing the rate of *Gli3* cleavage. The degradational term is due to normal *Gli3* degradation, as well as the conversion of *Gli3* to *Gli3R*. (4.1c) includes the increasing time due to *Gli3* to *Gli3R* conversion, as well as a degradational term of *Gli3R* at rate k_{deg} . Finally, (4.1d) shows the increase of *Ptc* due to the promoter transcriptional rate as well as the low, basal rate of transcriptional activation. It also shows a degradation of *Ptc* at a rate $k_{deg,P}$.

The parameters used for the model were somewhat simplified, such as the degradation rates for all Gli proteins to be the same. A detailed list of the parameters can be seen in 4.4 below, with a description of what each parameter represents.

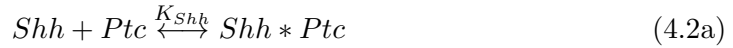
TABLE 1 Parameter values

Parameter	Description	Value/range
K_1, K_2 (Mizugishi et al., 2001)	Dissociation constant of Gli1 and Gli3 for Gli DNA binding site, respectively	8.3×10^{-10} M
k_{deg} (Chen et al., 1999)	Degradation rate constant for all Gli variants	0.009 min^{-1}
K_{Shh} (Fuse et al., 1999; Taipale et al., 2002)	Dissociation constant for Shh-Ptc binding	0.58–2.0 nM
K_{Ptc} (Taipale et al., 2002)	Half-maximal concentration of Ptc which inhibits Smo signaling	8.3×10^{-11} M
c (Keller, 1995)	Binding cooperativity	1
ε (Keller, 1995)	Transcriptional efficiency	0.5
r	Transcriptional repression	0.2
$k_{deg, P}$ (French and Lauffenburger, 1996)	Degradation rate constant for Ptc	0.09 min^{-1}
$v_{max, G}$	Maximum rate of Gli synthesis	2.4×10^{-10} M/min
$r_{bas, G}$	Basal rate of Gli synthesis	$v_{max, G}/100$
r_{g3b}	Basal rate of Gli3 synthesis	1.6×10^{-19} M ² /min
K_{g3rc}	Sensitivity constant of the conversion to signal strength	0.1
k_{g3rc}	Rate constant for the conversion of Gli3 to Gli3R	0.012 min^{-1}
$v_{max, P}$	Maximum rate of Ptc synthesis	7.5×10^{-10} M/min
$r_{bas, P}$	Basal rate of Ptc synthesis	$v_{max, P}/100$

Figure 4.4: Table of all parameter values and what they represent within the schematic. Table taken from [10]

4.3 Derivation of Signal

Using our knowledge of the Shh system, we see that *Shh* and *Ptc* reversibly react at a dissociation constant, K_{Shh} and so we are able represent this as follows:



We assume that on the gene transcription and protein synthesis time scale, a steady state value is achieved due to the rapid binding between Shh and Ptc, which may be described using a Scatchard relationship:

$$[Shh * Ptc] = \frac{[Shh][Ptc_{Total}]}{K_{Shh} + [Shh]} \quad (4.2b)$$

Due to binding of *Shh* to *Ptc*, the inhibition of *Smo* signaling from *Ptc* stops. "Signal" is defined as the fraction of uninhibited *Smo* concentration (amount no longer inhibited by *Ptc*) over the total amount of *Smo* concentration. Again, a Scatchard relationship model can be made of the *Smo* – *Ptc* interaction, and the expression for inhibited *Smo* is expressed as follows:

$$[Smo * Ptc] = \frac{[Ptc_{free}][Smo_{Total}]}{K_{Ptc} + [Ptc_{free}]} \quad (4.2c)$$

where $[Smo * Ptc]$ is the concentration of *Smo* inhibited by *Ptc*, $[Ptc_{free}]$ the concentration of *Ptc* not inhibited by *Shh*, $[Smo_{Total}]$ the concentration of total *Smo* and K_{Ptc} is the half maximal concentration of *Ptc* required to inhibit *Smo* activity.

As Signal is defined in such a way, and defining $[Smo_{free}]$ as the concentration of uninhibited Smo , we may mathematically model this as

$$Signal = \frac{[Smo_{free}]}{[Smo_{Total}]} = \frac{[Smo_{Total}] - [Smo * Ptc]}{[Smo_{Total}]} \quad (4.2d)$$

By substitution of (4.2b) and (4.2c) into (4.2d), we obtain the end expression for Signal:

$$Signal = \frac{[Smo_{free}]}{[Smo_{Total}]} = \frac{1 + \frac{Shh}{K_{Shh}}}{1 + \frac{Ptc}{K_{Ptc}} + \frac{Shh}{K_{Shh}}} \quad (4.2e)$$

where for simplicity, Smo is set to a constant value, as there are no reports that Smo is transcriptionally regulated by Shh signaling.

4.4 Shh as a Bistable Switch

The system network comprises of a positive feedback loop, contained within a negative feedback loop. Simpler models of autoregulatory transcription factor systems show bistability, so we are able to demonstrate that the Shh system functions as a bistable genetic switch, which relates to its ability to switch the fate of a cell at precise thresholds of Shh concentrations.

Gli is considered to be the most important output of the system, as $Gli1$ and $Gli2$ are considered to be integral parts of cellular responses due to the Shh signal occur, and so it is used to analyse the signalling system for bistability. It is also noted that the Shh concentration is given as a ratio to the Shh dissociation binding constant, K_{Shh} . This is due to a range of equilibrium dissociation binding constants found for the binding of Shh to Ptc , varying from values of 0.5nM to 2nM. A plot of Gli against time can be seen below:

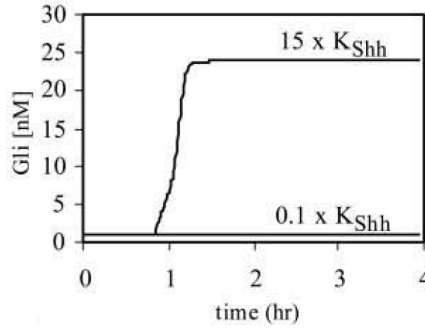


Figure 4.5: Gli as a function of time (hours) at a concentration of Shh equal to 0.1 and 15 times the Shh binding dissociation constant to Ptc , K_{Shh} . At 15 times K_{Shh} , the Gli curve is initially low until $t \approx 0.5$. Figure from [10].

As depicted in Figure 4.5, Gli concentrations are initially low for both levels of K_{Shh} , until time reaches an approximate value of 0.5. At this time for a Shh concentration 15 times the K_{Shh} constant, Gli production abruptly increases and reaches a new steady state value, which is approximately $24nM$. However, for a low value of 0.1 times K_{Shh} , Gli remains at a low steady state value of approximately $1nM$. This gives some evidence towards the switch-like behaviour of Shh . This is due to higher concentration levels above the threshold concentration exhibiting positive feedback, to which the "On" state of the system is achieved. This is explained by Shh -stimulated Gli production until Gli positively activates it's own production. This compares to low values showing an "Off" state, experienced by Gli transcription naturally occurring at a low value.

To look further into the behavioural properties of the switch, similarly to Figure 3.8 we can plot a bifurcation of how Gli changes as a function of the Shh/K_{Shh} concentration ratio.

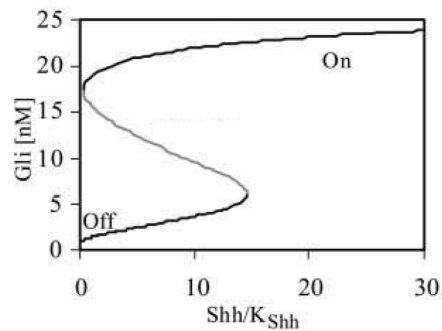


Figure 4.6: Gli as a function of Shh , showing hysteresis. The value of Gli can switch between two possible steady states dependent on Shh increasing or decreasing. Figure from [10].

As we can see from the above figure, there are two cases to consider. For Shh increasing from a lower value, Gli concentration increases gradually until Shh concentration reaches a threshold value of $Shh/K_{Shh} \approx 15$. This then causes the dramatic increase of Gli concentration to a value of approximately 22.5 from a value of approximately 6, causing the system to be "On". The second case is due to a decrease in Shh/K_{Shh} concentration from a high value to a low value. As depicted, the system stays within this "On" state until a very low threshold concentration of Shh/K_{Shh} is reached, much nearer to the value of zero. To conclude, this means that there are two points at which switching occurs, depending on if Shh/K_{Shh} is increasing or decreasing. In between these points, it's possible to obtain two steady state values of Gli (dark lines), with an unstable steady state value shown between these Gli concentrations (grey line).

4.5 Bifurcation Analysis of Disease Causes Within the Shh Network

Observations of the Shh network show that mutations within the system, or gene amplification are a causation to disease. Examples of such are the gene amplification of *gli1*, *Gli3* truncations, mutations leading to the fixation of a constant rate of Smo activation and *Ptc* mutations. This can cause the function to deteriorate even to a complete stop, which can be linked to the formation of cancer [12]. Bifurcation analysis was carried out for these examples to determine how sensitive these specific parameters are in breaking the switch of the system into an irreversible state.

4.5.1 Gene Amplification of *gli1*

The gene amplification of *gli1* would cause an increase in the constant $v_{max,G}$, so it is possible that we can mathematically represent this action with a bifurcation plot of $V_{max,G}$ as a function of Shh/K_{Shh} concentration.

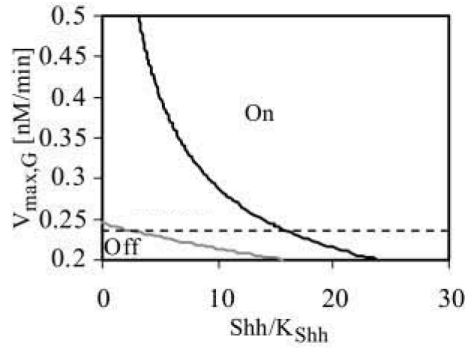


Figure 4.7: Bifurcation of *gli* promoter strength denoted by $V_{max,G}$ affecting the switch points of the system with varied Shh/K_{Shh} . Two curves (light and dark) represent the two steady state values, where the dashed line is the value of $V_{max,G}$ used in figure 4.6. Figure from [10].

The dashed line in figure 4.7 shows the value of $V_{max,G} = 0.24nM/min$ used in the calculation of figure 4.6, to which the system is in its “Off” state for a low initial concentration, until it increases to a threshold value of $Shh/K_{Shh} \approx 15$ where the system switches to an “On” state (high *Gli* concentration). As the concentration of Shh/K_{Shh} begins to decrease, it must reach another threshold point to be able to switch to it’s “Off” state again. This is when the dashed line intersects with the lighter curve, which is at $Shh/K_{Shh} \approx 2.5$.

However, if the value of $V_{max,G}$ increases (due to *gli1* amplification) above the threshold value of approximately $0.25nM/min$, problems occur. When Shh/K_{Shh} is increased to a value, which would cross the dark line, the system would turn to its “On” state. However, no matter how much there is a decrease in Shh/K_{Shh} concentration,

the system will always stay in its “On” state, creating an irreversible switch as opposed to a bistable one. The ramification that can ensue is that the system could be stuck in a state, which attempts to causes mitosis to occur repeatedly, which may initiate cell mutation into cancer.

4.5.2 Ptc and Smo Mutations

Mutations within Ptc can affect the inhibition it has on Smo, and it represented by the parameter K_{Ptc}^{-1} , with K_{Ptc} being the concentration of Ptc needed for half of the maximal inhibition. Figure 4.4 was calculated at a value of $K_{Ptc}^{-1} = 12nM^{-1}$.

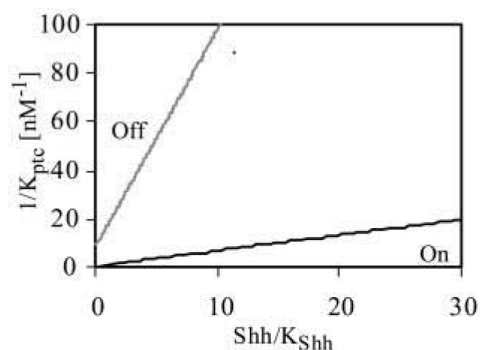


Figure 4.8: Bifurcation of Ptc potency to inhibit Smo activity, K_{Ptc}^{-1} as a function of Shh/K_{Shh} concentration. Exhibits bistability for only a small range of values of K_{Ptc}^{-1} . Figure from [10].

As we can see, for values of K_{Ptc}^{-1} between approximately 10 and $20nM^{-1}$, as Shh/K_{Shh} increases from a low initial value, the system will eventually turn “On” when it intersects with a value of the dark curve. When the Shh/K_{Shh} value decreases from this higher value, the system will again switch to its “Off” state when it intersects with the lighter curve. Problems arise when K_{Ptc}^{-1} decreases below this threshold point of around $10nM^{-1}$, to which breaks the switch like behaviour forcing the system into an irreversible state once it is turned “On”. This again, would initiate cell transformation and cancer.

4.5.3 Gli3 Truncations

Through the mutation of *Gli3* proteins, it has been clinically observed to have a link with some cancers due to the protein being truncated. This can be mathematically modelled as a change in the dissociation constant of *Gli3* for *Gli* DNA binding site, K_2 .

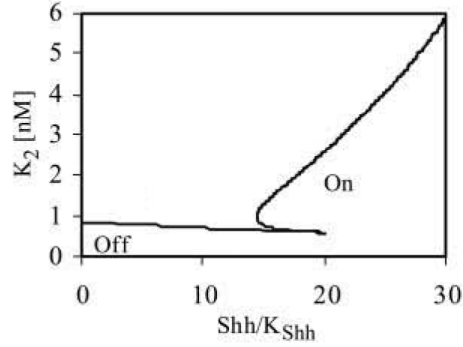


Figure 4.9: Bifurcation of K_2 , the binding dissociation constant of *Gli3* for its DNA site. Minor changes in K_2 values can cause an irreversible switch and hence is a highly sensitive parameter. Figure from [10].

For example, as shown in figure 4.9, for lower initial levels of Shh/K_{Shh} the state of the system is “Off” until it reaches a value of approximately 15 for when $K_2 \approx 0.8$. This system will then switch “On” and will remain on until it intersects the curve close to a Shh/K_{Shh} value of zero. However, even with a very slight increase of K_2 , the system will remain in its “On” state once a high enough concentration of Shh/K_{Shh} has been established.

Not all parameters are as sensitive to the system however, which is the case for the basal rate of *Ptc*, $r_{bas,P}$.

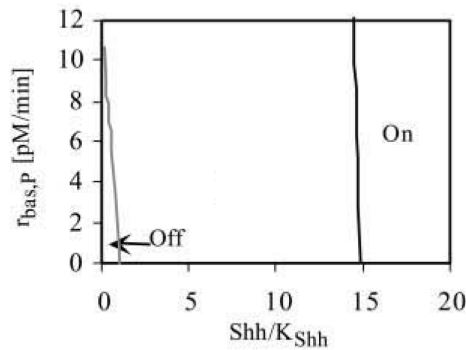


Figure 4.10: Basal rate of *Ptc*, $r_{bas,P}$ as a function of Shh/K_{Shh} . Even with a significant change in $r_{bas,P}$, bistability still arises as the system is able to switch between two state with an increase/decrease of Shh/K_{Shh} concentration. Figure from [10].

From values of $r_{bas,P}$ between zero and approximately 11, the system exhibits hysteresis. For values above 11 however the system’s switch like behaviour will break and stay in its “On” state.

A follow up study develops the model further by modelling the spatial and temporal evolution of the *Shh* signal using partial derivatives [12].

Chapter 5

Shh and Development of the Spinal Cord

5.1 Spinal Cord Ventral Patterning

Another separate model was used to mathematically inspect the interaction between Sonic Hedgehog concentration and the fibroblast growth factors (FGF) found at the caudal end of the neural plate, exposing themselves to neural progenitors (differentiable neurons) [13]. These FGF produce signals which act as inhibitors to differentiation, causing a steady value of the amount of undifferentiated neural progenitors that are necessary for a complete spinal cord seen in figure 5.1. FGF also inhibits the expression of many transcriptional factors which give cells their identity, to which after the local concentration of FGF around cells decreases enough, they cells can then mature and express different transcriptional factors [14].

From this model, Shh binds to Patched1 (*Ptch1*), reducing the inhibition of *Ptch1* on *Smo*. This promotes *Smo* activity, which in turn promotes the activator forms of Gli transcription factors, while inhibiting the repressor forms. This cascade goes on to activate downstream target genes responsible for cell identity. Many other additional components are involved within intermediate steps of the process, but the basic core components is what is important here. One feedback loop in particular is the transcriptional activation of *Ptch* when signalling is active acts in two ways; to reduce signalling response to specific *Shh* concentration and to control the gradient concentration of extracellular *Shh* by isolation [15].

It has been experimentally shown that FGF activates *Ptch2* activity, which inhibits *Shh* signaling. *Ptch2*, a receptor of *Shh* works similarly to *Ptch1*. This receptor is a part of a negative feedback loop, increasing the amount of *Shh*-dependent ventral neural progenitor cells [16].

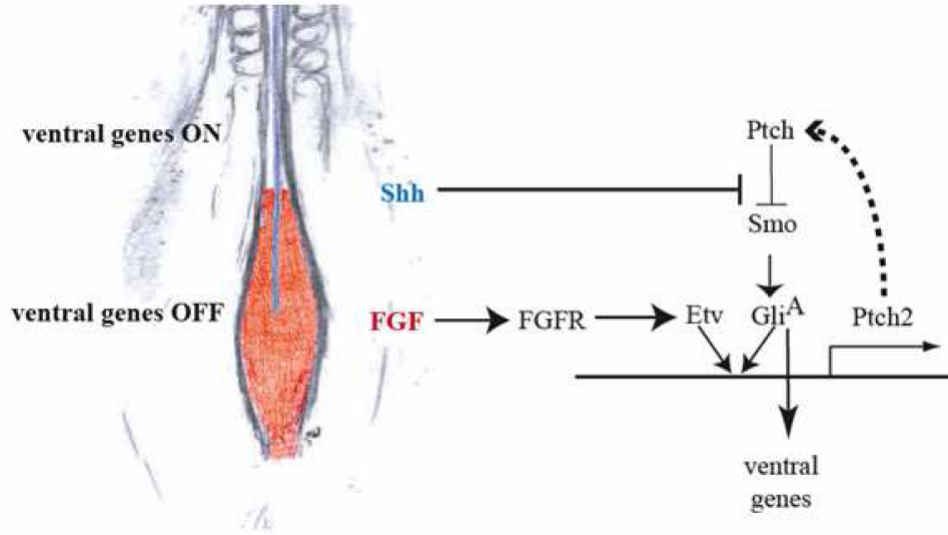


Figure 5.1: Schematic of FGF influence on the Shh signal. Figure from [19].

The aim of this model was to investigate how FGF and Shh interact and its effect on the Shh pathway, which is done by mathematically modelling the core Shh network with a simplified three ODE system. Then, to analyse what effect each parameter has on the pathway, especially with the negative feedback interaction. Finally, to include FGF signalling into the mathematical model to determine its effect on the network in greater detail. What is also of interest is to determine whether the stable steady states have at least one stable value for all fixed values of Shh_T greater than zero.

5.2 Revised Model of Core Shh Signalling System

The reason behind the revision of the model first discussed in previous studies [10], [11] is to use only the essential elements of the Shh signalling pathway and to simplify other interactions within as currently their mechanisms are not fully understood. Whereas bistability was established in the more complex and detailed system, experimental results do not support bistability as a key feature of the system [17] and so the term that provides such bistability was excluded. Here we are not considering temporal changes of Shh concentration in space and time, but we are interested in the change of Smo , $Ptch$ and $Ptch - Shh$ concentrations at a fixed Shh concentration value.

By inspection of our schematic in Figure 4.2, we are able to mathematically model this system using methods seen in chapters 1 and 2. For simplicity, transcriptional inhibition and activation effects are expressed through Hill equations.

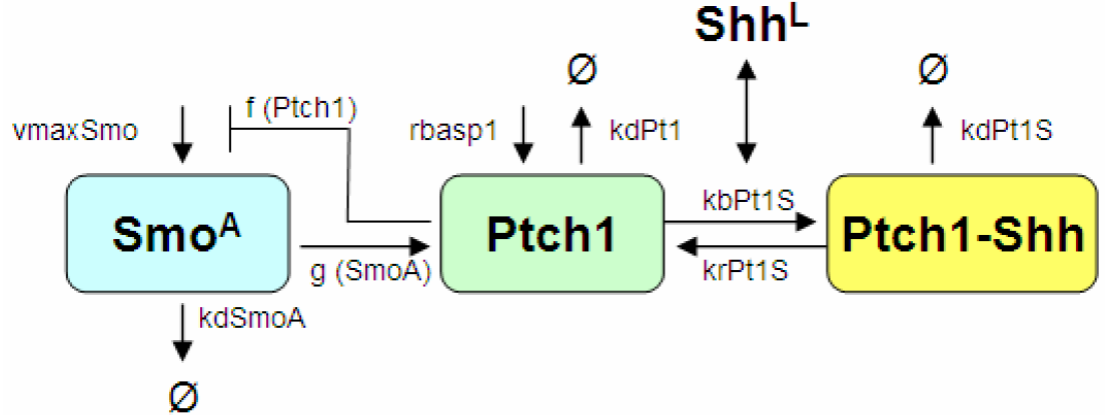


Figure 5.2: Schematic of the revised Shh signalling system. *Shh* binds to *Ptch1*, releasing the inhibition of *Ptch1* on *Smo* activity. Figure from [19].

$$\frac{dSmo^A}{dt} = v_{max}Smo \frac{k_1^{n_1}}{k_1^{n_1} + (Ptch1 + Ptch2)^{n_1}} - kdSmo^A Smo^A \quad (5.1a)$$

$$\begin{aligned} \frac{dPtch1Shh}{dt} &= kbPt1S(ShhT - Ptch1Shh)Ptch1 - krPt1SPtch1Shh \\ &\quad - kdPt1SPtch1Shh \end{aligned} \quad (5.1b)$$

$$\begin{aligned} \frac{dPtch1}{dt} &= r_basp1 + ksPt1 \frac{Smo^{A n_2}}{Smo^{A n_2} + k_2^{n_2}} - kdPt1Ptch1 + krPt1SPtch1Shh \\ &\quad - kbPt1SPtch1(ShhT - Ptch1Shh) \end{aligned} \quad (5.1c)$$

Note that in the first differential equation, the variable *Ptch2* is set to be equal to zero for the simpler ODE system, but will be implemented later when we include FGF signalling. In addition, the *Smo* is assumed to be produced in an active form, *Smo^A*, causing the transcriptional activation of target genes. Assumptions are also made that there is a fixed total amount of *Shh*, which interacts with *Ptch* receptors in a reversible manner. To simplify the model so that transcription and translation terms are combined, components of the system represent the proteins synthesised from their corresponding mRNAs, and so a quasi-steady state assumption has been made for mRNAs [18].

For the change of *Smo^A* concentration, we have a production term at a rate of $v_{max}Smo$, the maximal rate of *Smo* synthesis, multiplied by a Hill function of k_1 and *Ptch1*. Also there is a decay term due to the degradation of *Smo^A* at a rate $kdSmo^A$. Next, the change in *Ptch1Shh* concentration includes a production term due to the

activation from the amount of unbound Shh (seen as $ShhT - Ptch1Shh$) binding with available $Ptch1$ to create a $Ptch1Shh$ complex. The decay terms are due to the release of $Ptch1Shh$ back into its constituents at a rate $krPt1S$ and due to the degradation of $Ptch1Shh$ at a rate $kdPt1S$. Finally, the third differential equation represents the change in $Ptch1$, with promotional terms due to the basal rate of $Ptch1$ synthesis, the release of $Ptch1Shh$ and the Hill function of Smo^A and $k_2^{n_2}$. The decay terms come from the degradation of $Ptch1$ and the formation of the $Ptch1Shh$ complex at the rate $kbPt1S$.

5.3 Parameter Values and their Effects

The table below includes a description and value of each parameter within the mathematical model, taken from [19], with initial conditions of $[Shh] = 1$; $[Ptch1] = 1$; $[PtchShh] = 0$; $[Smo^A] = 1.0nM$.

Parameter	Value	Description
$v_{max}Smo$	$0.24nM/min$	Maximum rate of Smo synthesis
k_1	$0.8nM$	Concentration of $Ptch$ required to lower Smo to half of it's maximal activity
n_1	2	-
$kdSmoA$	$0.07min^{-1}$	Degradation rate constant for $SmoA$
$kbPt1S$	$1.2min^{-1}$	Binding rate constant for $Ptch1Shh$
$krPt1S$	$0.696min^{-1}$	Release rate constant for $Ptch1Shh$
$kdPt1S$	$0.07min^{-1}$	Degradation rate constant for $Ptch1Shh$
$rbasp1$	$0.0075nM/min$	Basal rate of $Ptch1$ synthesis
$ksPt1$	$0.12nM/min$	Maximum rate of $Ptch1$ synthesis
n_2	2	-
k_2	$0.2nM$	Concentration of $SmoA$ required to increase $Ptch$ to half of it's maximal level
$kdPtch1$	$0.04min^{-1}$	Degradation rate constant for $Ptch1$
γ	1	-

Table 5.1: Table of parameters used to mathematically model the system taken from [19].

By using the model and parameter values from the table above, a sensitivity analysis can be made to determine which parameters hold the most influence of the response of Smo activity to the presence of surrounding Shh concentration. Two specific cases are the change of maximal production rates and degradation rates of Smo concentration, while others did not alter the maximal Smo concentration reached significantly enough.

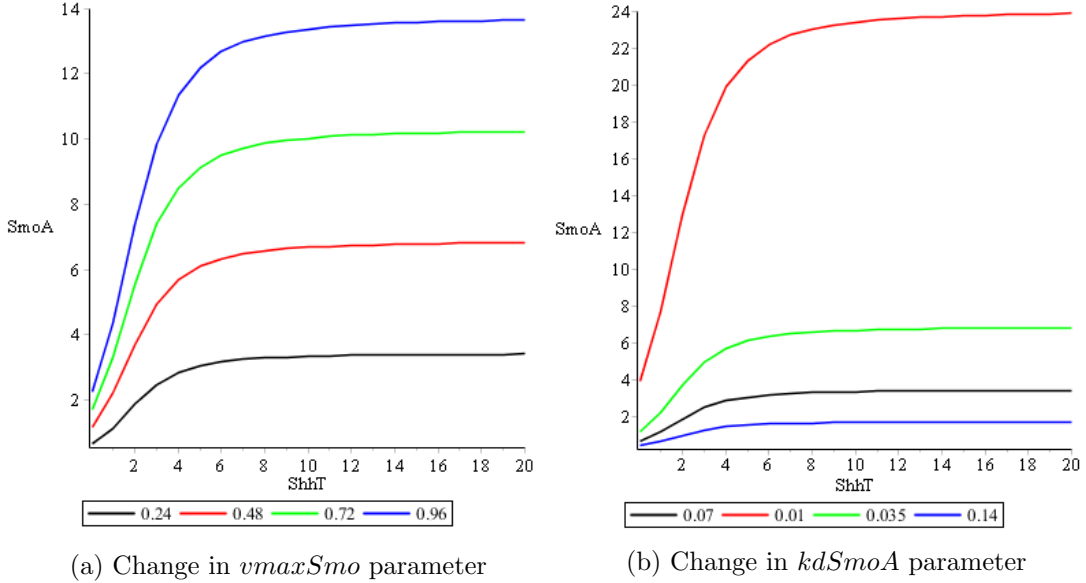


Figure 5.3: Smo concentration as a function of a fixed $ShhT$ concentration. (A): Change in $vmaxSmo$ affecting the maximal steady state value of Smo . (B): Change in $kdSmoA$.

As seen, from (A) we have an increase in maximal Smo concentration with an increase of the parameter $vmaxSmo$, and decrease with a reduced value of the parameter. Also a similar effect in (B), with a change in degradation rate $kdSmoA$. However, increase from a lower value of $kdSmoA$ has more of a profound effect on the steady state value of $SmoA$ compared to an increase from a higher value. Also by inspection, we see that once the fixed $ShhT$ concentration reaches a value of around $5nM$, the change in steady state values of $SmoA$ does not change significantly, and actually begins to reach a maximal value for the respective parameter values. This trait seems to link to the saturated effect of extracellular $ShhT$ concentration, so that no matter how much more the concentration of $ShhT$ is increased, the amount of Smo concentration will remain at this maximal steady state value. The shape of the curves are also considered to be sigmoidal, implying that the reaction is cooperative.

To check whether this system will remain in a steady state value under the default parameter values given in Table 5.1, we will use the mathematical software *Maple* to develop stability analysis for this three variable system, to determine whether there will always be at least one steady state value. However, it has proven too difficult to show analytically how the system will always contain one stable equilibrium point. Even with assumptions that the variables in question and the parameter $ShhT$ are positive, it isn't possible to analyse the eigenvalues of characteristic polynomial unless the values are stated. Using the default parameter values we are able to at least analyse the system for specific equilibria. Hence, we obtain the equilibrium points of the system found by setting equations (5.1a-c) equal to zero. Note that six equilibria were found, however four of which were complex points, and one had a negative value for

the variable $Ptc1$ which is considered to be impossible to obtain in a biological sense (can only have real, positive concentrations) and so only one fixed point is considered. Therefore, by conducting a few tests for values of $ShhT$ at 1, 5, 10, 20 and $30nM$ to see if these fixed points found respective to the stated $ShhT$ values, we show they are indeed stable. The respective fixed points are as follows:

$$SmoA = 1.143042472, Ptc1Shh = 0.6392713705, Ptc1 = 1.131233264 \quad (5.2a)$$

$$SmoA = 3.049618446, Ptc1Shh = 1.532080006, Ptc1 = 0.2820070067 \quad (5.2b)$$

$$SmoA = 3.341109043, Ptc1Shh = 1.685871696, Ptc1 = 0.1294360708 \quad (5.2c)$$

$$SmoA = 3.408512874, Ptc1Shh = 1.754176460, Ptc1 = 0.6137017080 \quad (5.2d)$$

$$SmoA = 3.419955757, Ptc1Shh = 1.775432208, Ptc1 = 0.4015358420 \quad (5.2e)$$

Now, to determine their stability again we will check the eigenvalues produced from the 3x3 Jacobian matrix.

$$J = \begin{bmatrix} -kdS & 0 & -\frac{Vm k1^{n1} (Ptc1+Ptc2)^{n1} n1}{(k1^{n1}+(Ptc1+Ptc2)^{n1})^2 (Ptc1+Ptc2)} \\ 0 & -kbP Ptc1 - kdP - kr & kbP (ShhT - Ptc1Shh) \\ \frac{ks SmoA^{n2} n2}{SmoA (SmoA^{n2} + k2^{n2})} - \frac{ks (SmoA^{n2})^2 n2}{(SmoA^{n2} + k2^{n2})^2 SmoA} & kbP Ptc1 + kr & -kdP - kbP (ShhT - Ptc1Shh) \end{bmatrix} \quad (5.3)$$

The respective eigenvalues for the equilibria points given in order are a follows:

$$\begin{aligned} \lambda_{1,1} &= -0.700199794085307 + 0.217104332133987i, \\ \lambda_{1,2} &= -0.700199794085307 - 0.217104332133987i, \\ \lambda_{1,3} &= -2.55631431358294, \end{aligned} \quad (5.4a)$$

$$\begin{aligned} \lambda_{2,1} &= -0.700043280267235 + 0.334357803993192i, \\ \lambda_{2,2} &= -0.700043280267235 - 0.334357803993192i, \\ \lambda_{2,3} &= -5.26590374494655, \end{aligned} \quad (5.4b)$$

$$\begin{aligned} \lambda_{3,1} &= -0.700010021392614 + 0.136097285387602i, \\ \lambda_{3,2} &= -0.700010021392614 - 0.136097285387602i, \\ \lambda_{3,3} &= -10.8982752407215, \end{aligned} \quad (5.4c)$$

$$\begin{aligned}
\lambda_{4,1} &= -0.700002334159351 + 0.609855858830547i, \\
\lambda_{4,2} &= -0.700002334159351 - 0.609855858830547i, \\
\lambda_{4,3} &= -22.7346319881681,
\end{aligned} \tag{5.4d}$$

$$\begin{aligned}
\lambda_{5,1} &= -0.700001009549898 + 0.391866965841520i, \\
\lambda_{5,2} &= -0.700001009549898 - 0.391866965841520i, \\
\lambda_{5,3} &= -34.6836654490900
\end{aligned} \tag{5.4e}$$

As we can see, all real parts for all eigenvalues are negative and so all respective fixed points are stable.

5.4 Model including FGF signalling

Moving on from the core *Shh* signalling system, we are now going to introduce FGF signalling into the mathematical model. Exposure of FGF to cells when *Shh* signalling is active has been experimentally shown to promote the activity of *Ptch2*, which can alter the response of cells to *Shh* signalling. This is upregulated by *Shh* signalling, hence is a part of a negative feedback loop within the system. By extending the system of three ODEs to five ODEs, we are able to describe the dynamics of the five variables in question, Smo^A , *Ptch1*, *Ptch1 - Shh*, *Ptch2* and *Ptch2 - Shh*.

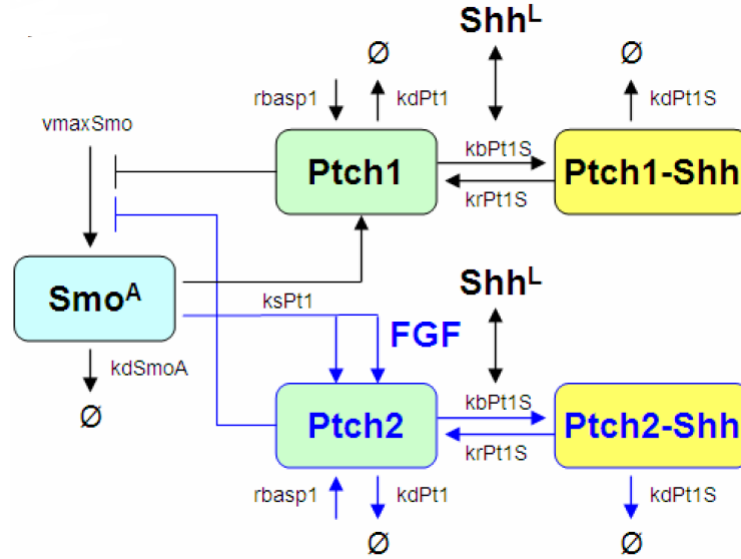


Figure 5.4: Basic schematic diagram of Sonic hedgehog signalling system, now with FGF incorporated into the model. Figure from [19].

The additional equations that add to (5.1a)(5.1b)(5.1c) are the following:

$$\begin{aligned} \frac{dPtc2Shh}{dt} = & kbPt1S(ShhT - Ptc2Shh)Ptc2 - krPt1SPtc2Shh \\ & - kdPt1SPtc2Shh \end{aligned} \quad (5.1d)$$

$$\begin{aligned} \frac{dPtc2}{dt} = & rbasp1 + ksPt1(\gamma + FGF) \frac{SmoA^{n2}}{SmoA^{n2} + k2^{n2}} - kdPt1Ptc2 \\ & + krPt1SPtc2Shh - kbPt1SPtc2(ShhT - Ptc2Shh) \end{aligned} \quad (5.1e)$$

Here, we have for (5.1d) the production term due to free *Shh* outside of the cell combining with *Ptc2* to create *Ptc2Shh* at a rate of $kbPt1S$. The two decaying terms are due to the conversion of *Ptc2Shh* back into *Ptc2* and *Shh* at a rate $krPt1S$, and the degradation of *Ptc2Shh* at a rate $kdPt1S$. For (5.1e), we have three production terms, which are respectively due to the basal synthesis of *Ptc2* at a rate $rbasp1$, the promotion of *Ptc2* concentration due to FGF signalling at a rate $ksPt1$ and the release of *Ptc2Shh* into *Ptc2* and *Shh* separately. The two respective decay terms are due to the degradation of *Ptc2* and the conversion of *Ptc2* into the *Ptc2Shh* complex when combined with *Shh*.

As stated previously that *Ptc2* inhibits *Smo* activity, then we would like to see what effect the increase in FGF concentration will have on the amount of *Shh* required to promote *Smo*. By solving the system for *SmoA* steady state values at various fixed *ShhT* concentrations, we are able to plot *SmoA* concentration as a function of *ShhT*:

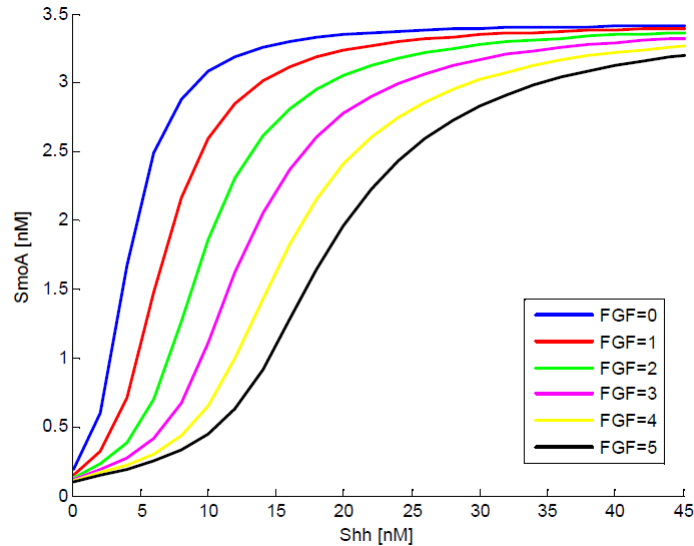


Figure 5.5: *Smo* as a function of *ShhT* concentration with various fixed levels of FGF in nM. All other parameter values were set to a default value, taken from the parameter table. Figure from [19].

The response of *SmoA* to *ShhT* concentration is reduced with an increased presence

of FGF concentration, which is more evident for mid range levels of *ShhT* concentration, rather than low or high *ShhT* concentrations. There is also a slight change in the maximal steady state *Smo* concentration with an increase in FGF concentration. However, it is only minor but appears to be expressed more so for higher levels of FGF.

Chapter 6

Conclusion

In this project, we have studied the dynamics of biochemical reactions and the dynamics of feedback loops within biological systems, applying to the Sonic Hedgehog signalling system. We have developed the understanding of how Michaelis-Menten kinetics applied to biochemical reactions, in both a single substrate and cooperative substrate sense, indicating how simplifications can be made to obtain the simple sigmoidal case for cooperative reactions. By using the quasi steady state assumption, we were able to simplify the models to obtain an equation of the rate of production formation (1.8c), otherwise known as the velocity of the reaction. By plotting this equation against substrate concentration s , we were able to see mathematically that enzymes work at a maximal rate after a specific threshold concentration of s , no matter the increase of s . Also by nondimensionalisation, we were able to discover how the dynamics of a reaction occurs during the initial transient time scale and the longer (relaxation) time scale, which was then plotted as a phase portrait in Maple. We also established that a Hill equation can be found for multi-substrate reactions, by simplifying the resulting rate equation.

Furthermore, we have established an understanding of the dynamics of regulatory feedback loops with an insight into yeast glycolysis, and further detail into a generic example of mutual inhibition. By modelling the simplified system, we were able to use default parameters given to create time plots of how concentrations of proteins change. Specifically, we saw that with a change in the parameter K_m , we obtained oscillatory behaviour and damped oscillations for respective values of 13 and 20. We then obtained fixed points of the system and by numerically analysing the resulting Jacobians and eigenvalues using maple, we determined the stability of these points using stability theory. The conclusion for the value $K_m = 13$ was that we had unstable spiral behaviour, but once a phase portrait was plotted we saw that a limit cycle existed due to the Poincaré-Bendixon theorem. We concluded that this related to the system “overshooting” the production of both proteins when they are respectively low, causing this oscillatory behaviour. During the analysis of the mutual inhibition example, we

established an understanding of how hysteresis can occur within a system, and solidifying that statement by analysing the three fixed points to obtain two stable and one unstable point. Also by analysing the bifurcation plots for mutual inhibition, we saw how the system would switch to its “on” state with an increase in signal concentration, and back to its “off” state with a decrease in signal concentration. Similarly, we established that for mutual activation that the system would be unable to turn “off” after a decrease in signal concentration causing what is known as an irreversible switch.

This knowledge was then used to consider the effect on the Sonic Hedgehog signalling system, and concluded that it is possible to obtain an irreversible switch under parameter changes from the Sonic Hedgehog signalling pathway model. Notable effects were changes in parameters $V_{max.G}$, K_{Ptc}^{-1} and K_2 , highlighting the causation of *gli1* over transcription, Patched and Smoothed protein mutations and Gli3 truncations respectively which possibly lead towards disease such as cancer. Another simpler model was taken into consideration to analyse the effects that FGF has on the system, and excluding bistability as it was experimentally found not to have a key role in the system. Analysis of the stability of the simpler three variable model was determined to not be possible numerically, and so for the specific range of Sonic Hedgehog concentrations stated, the system was found to be stable. For the five variable model which included FGF signalling, it was shown that FGF alters the total amount of Sonic Hedgehog concentration required to activate *SmoA* production by increasing the threshold value. This threshold value would also increase higher with an increase of FGF concentration, although only a slight decrease on the maximal *SmoA* value attained was shown. Further research can be done, by considering spatio-temporal effects of Shh concentration within the Sonic Hedgehog signalling system to give a better insight into how the system works.

From this study, we conclude that biochemical reactions can indeed be modelled mathematically and used to explain abnormalities within a biological system (specifically the Sonic Hedgehog signalling system) where others may not detect why they appear. In addition, FGF does alter the Sonic Hedgehog signalling system by decreasing the response of the Sonic Hedgehog signal which is useful for patterning of the neural tube.

Bibliography

- [1] Leah Edelstein-Keshet “**Mathematical Models in Biology**”, (1988).
- [2] J.D Murray “**Mathematical Biology: I. An Introduction**”, **Third Edition**, (2002).
- [3] Martin Bier, Barbara M. Bakker, and Hans V. Westerhoff “**How Yeast Cells Synchronize their Glycolytic Oscillations: A Perturbation Analytic Treatment**”, (2000).
- [4] John J Tyson, Katherine C Chen and Bela Novak “**Sniffers, buzzers, toggles and blinkers: dynamics of regulatory and signaling pathways in the cell**”, (2003).
- [5] Eric A. Sobie “**An Introduction to Dynamical Systems**”, (2011) - <http://stke.sciencemag.org/content/suppl/2011/09/16/4.191.tr6.DC1>
- [6] Eric A. Sobie “**Bistability in Biochemical Signaling Models**”, (2011) - <http://stke.sciencemag.org/content/suppl/2011/09/23/4.192.tr10.DC1>
- [7] James E Ferrell Jr “**Self-perpetuating states in signal transduction: positive feedback, double-negative feedback and bistability**”,(2002).
- [8] Alex Mogilner, Roy Wollman and Wallace F. Marshall **Quantitative Modeling Review in Cell Biology: What Is It Good for?**, (2006).
- [9] Scott F. Gilbert “**Developmental Biology**”, **Tenth Edition**, (2014).
- [10] Karen Lai, Matthew J. Robertson, and David V. Schaffer “**The Sonic Hedgehog Signaling System as a Bistable Genetic Switch**”, (2004).
- [11] Krishanu Saha and David V. Schaffer Development 133, 889-900. “**Signal dynamics in Sonic hedgehog tissue patterning**”, (2006).
- [12] Ariel Ruiz i Altaba, Pilar Sánchez and Nadia Dahmane ”**GLI AND HEDGEHOG IN CANCER: TUMOURS, EMBRYOS AND STEM CELLS**”, (2002).

- [13] Diez del Corral R., Breitkreuz, D.N, and Storey, K.G. **“Onset of neuronal differentiation is regulated by paraxial mesoderm and requires attenuation of FGF signalling”**, (2002).
- [14] Diez del Corral R., Olivera-Martinez I, Goriely A, Gale E, Maden M, and Storey K. **“Opposing FGF and Retinoid Pathways Control Ventral Neural Pattern, Neuronal Differentiation, and Segmentation during Body Axis Extension”**, (2003).
- [15] Dessaud E, McMahon AP, Briscoe J. (2008). **“Pattern formation in the vertebrate neural tube: a sonic hedgehog morphogen-regulated transcriptional network”**, (2008).
- [16] Holtz AM, Peterson KA, Nishi Y, Morin S, Song JY, Charron F, McMahon AP, Allen BL. **“Essential role for ligand-dependent feedback antagonism of vertebrate hedgehog signaling by PTCH1, PTCH2 and HHIP1 during neural patterning”**, (2013).
- [17] Balaskas N, Ribeiro A, Panovska J, Dessaud E, Sasai N, Page KM, Briscoe J, Ribes V. **“Gene Regulatory Logic for Reading the Sonic Hedgehog Signaling Gradient in the Vertebrate Neural Tube”**, (2012).
- [18] Polynikis A, Hogan SJ, di Bernardo M. **“Comparing different ODE modelling approaches for gene regulatory networks”**, (2009).
- [19] Lopez P.R, Diez del Corral R., Biophysics Master UAM Instituto Cajal **“Mathematical modeling of the Sonic hedgehog pathway and its modulation by Fibroblast Growth Factor signalling in the developing spinal cord”**, (2013).